# CFD STUDY OF DIFFUSER GEOMETRY EFFECTS ON DIFFUSER AUGMENTED WIND TURBINE PERFORMANCE

BY

ERIC SAM NORTRUP

THESIS

Submitted in partial fulfillment of the requirements
for the degree of Master of Science in Mechanical Engineering
in the Graduate College of the
University of Illinois at Urbana-Champaign, 2010

Urbana, Illinois

Advisor:

Professor Jimmy Hsia

# ABSTRACT

This thesis aims to explore the performance limits of diffuser augmented wind turbines. Many studies of this topic have been performed in the past. Limiting assumptions and manufacturing concerns have forced the majority of previous studies to stray away from finding optimal performance in favor of economical construction. A momentum theory exists that shows the Betz limit can be exceeded by diffuser augmented wind turbines. In a multistage optimization study, geometry factors are considered and compared based on resulting power coefficients. In the final phase of the study a diffuser is chosen and compared to previously designed and tested diffusers. The new diffuser is the first to consider performance based not on rotor area, but on diffuser exit area. This diffuser exceeds the Betz limit based on diffuser exit area without considering the beneficial effects of blade tip vortices that have been found in multiple real-world tests.

# ACKNOWLEDGMENTS

The author wishes to express sincere appreciation to Professors Hsia for his assistance in the preparation of this manuscript and for agreeing to work with a non-traditional, off-campus thesis project. In addition, special thanks to David Shelander whose words of encouragement and passion for continually learning and growing inspired this study. Thanks also to Dr. Jack Yan who has always fully accommodated the requirements of my graduate studies with a flexible work schedule. And finally, thanks to my girlfriend and family who have helped me through the sometimes trying process of earning my Master's Degree.

TABLE OF CONTENTS

# LIST OF SYMBOLS

| | |
|---|---|
| a | Axial Flow Interference Factor |
| $A_d$ | Disc Area |
| $A_{exit}$ | Diffuser Area |
| $A_w$ | Wake Area |
| $A_\infty$ | Area Far Upstream |
| $C_d$ | Drag Coefficient |
| $C_t$ | Thrust Factor |
| $C_{t,amb}$ | Ambient Thrust Coefficient |
| $C_p$ | Power Coefficient Based on Rotor Area |
| $C_{p,Betz}$ | Power Augmentation |
| $C_{p,exit}$ | Specific Power Coefficient |
| $C_{pmax}$ | Betz Limit |
| $C_{p,w}$ | Wake Pressure Coefficient |
| $F$ | Force |
| $L$ | Characteristic Length |
| $p_{exit}$ | Pressure at Diffuser Exit |
| $p_w$ | Pressure in Wake |
| $p_1$ | Pressure Upstream of Rotor |
| $p_2$ | Pressure Downstream of Rotor |
| $p_\infty$ | Pressure Far Upstream |
| $P_c$ | Power Available |
| $P_w$ | Power of the Wind |
| $U_d$ | Velocity at Disc |

| | |
|---|---|
| $U_w$ | Wake Velocity |
| $U_\infty$ | Velocity Far Upstream |
| $V$ | Flow Velocity |
| $\beta$ | Diffuser Exit Area Ratio |
| $\nu$ | Kinematic Viscosity |
| $\rho$ | Density |
| $\gamma$ | Exit Backpressure Ratio |
| dP | Pressure Difference |
| $R_e$ | Reynolds Number |
| DAWT | Diffuser Augmented Wind Turbine |
| EAR | Exit-Area-Ratio |
| HAWT | Horizontal-Axis Wind Turbine |
| VAWT | Vertical-Axis Wind Turbine |

# CHAPTER 1: INTRODUCTION

Wind power generation is a rapidly growing industry and an important source of energy. Worldwide wind power capacity is currently over 158 GW [1]. It is estimated by industry experts that by the year 2014 this capacity will be greater than 400 GW. In the United States more than 35 GW of wind power capacity are currently in service. This 35 GW only makes up about 2% of the current US energy needs [1]. 2% is a surprisingly small amount, but it also indicates that there is substantial room for growth. In addition, rising oil prices and an unstable Middle East are ensuring that alternative energies make their way into the mainstream of energy production. Figure 1.1 shows the cumulative installed capacity for wind power worldwide.

One limitation of wind power generation is the low kinetic energy of the wind. While the average wind speed at a potential wind farm site is critical, wind energy is, in general, a very diffuse energy. This is due to the low density of air as compared to, for example, water, which is 800 times denser. In order to capture a significant amount of power and make wind power more economically viable, wind turbine sizes have been growing larger and larger. Current land based windmill farms have turbines with diameters of around 100m. These have become so large that they are becoming increasingly difficult to transport to an installation site.

The Betz limit 0.593 is the theoretical limit on the amount of energy a bare wind turbine can collect. Great deals of research and development time have been devoted to optimizing wind turbine blade designs. Mechanical losses due to friction and drag result in real world performance lower than this limit. The most efficient modern horizontal wind turbines capture roughly 70 to 80% of this limit or 40 to 45% of the wind's potential energy.

### 1.1. Wind Power Beginnings

The use of wind power far precedes the invention of and subsequent growing demand for electricity. The earliest windmills were literally mills. In fact, the first wind mills were seen in ancient Persia and were used to grind grains [2]. These first windmills could also be considered the first augmented windmills. They were Savonius, or drag based vertical axis wind turbines, VAWTs, that incorporate scoops or sails and is partially contained in an outer structure that channels the wind [3]. From this it is clear that the idea of increasing the energy density of wind is not a new one.

Horizontal axis wind turbines or HAWTs later gained popularity in Europe. They became widely used for grinding grain and pumping water [3]. Since the first windmills there have been vast arrays of designs for increasing their power output. One of the more prominent methods is

the addition of a diffuser around or behind a conventional HAWT creating a diffuser augmented wind turbine, DAWT. A Diffuser used to augment an HAWT can create a large low pressure zone in the wake of the turbine that pulls more air at higher velocity past the turbine. This energy dense air that is passing through the diffuser and turbine has increased kinetic energy and, therefore, the amount of energy captured by the turbine can be significantly increased.

While this topic has been investigated numerous times, due to the complex nature of the problem there has been limited success in parametrically evaluating the features that impact effectiveness or augmentation. There are, in fact, a great deal of parameters that can be examined. One way to make a study more manageable is to set strict limits on parameter variation. In many studies, the initial assumptions and range limits have been so restrictive as to limit the potential for augmentation. The current study is specifically targeting and attempting to exceed the long established Betz limit based on diffuser exit area and not rotor diameter. This is done by parametrically making geometry changes to optimize a diffuser for a given cross-sectional area and length. This thesis looks at diffuser geometry with limited initial restrictions in an attempt to find the limits of attainable augmentation and DAWT efficiency.

## 1.2. Scope of the Research

### 1.2.1. Limitations of the study

Due to budget limitations this study is strictly performed through computer simulation. A commercially available computational fluid dynamics, CFD, code is used to simulate wind tunnel testing. Multiple geometry factors are varied. Power coefficients and specific power coefficients are compared as performance criteria. In addition pressure, velocity, and thrust coefficient readings were taken to expose any possible trends or critical correlations. In order to ensure accuracy and comparability with previous studies, designs that were previously built are analyzed and results are compared back to the empirical findings.

### 1.2.2. Unique Aspects

Many of the previous studies on this topic have incorporated very limiting initial constraints. Admittedly, many of these constraints are necessary to attempt to produce a cost effective and commercially viable end product. Instead of focusing strictly on producibility and cost effectiveness, this study focuses on optimizing power augmentation versus diffuser exit area. It is the assertion of the author that understanding the limits of performance and effects of geometry changes will be a valuable engineering design reference. It will allow for a more informed decision making process when manufacturability or production cost reduction choices must be made. Some of the most prominent prior designs are

examined in an attempt to explore the bounds of augmentation in a CFD format. There are two previous studies, in particular, that have had some level of success in demonstrating increased performance level. These designs are to this date the most efficient at augmenting a wind turbine based on diffuser area. Some of the assumptions made during these studies are loosened to explore diffuser augmentation possibilities or limitations.

### 1.2.3. Impact of Study

The structural support associated with mounting a land based DAWT makes the design cost prohibitive [4]. Mounting a DAWT 150 to 200 ft in the air, while possible, would require massive structural support. This is due to the much higher drag coefficient of the diffuser as compared to a feathered traditional turbine of similar area. It would require a very robust support structure in the case of extreme winds. One area where this design could be highly effective is in ocean based wind farms. Due to the lack of obstacles and lower turbulence levels, ocean based wind turbines can be mounted much nearer to the water surface. In addition, the underwater supports of an ocean based wind farm could be linked to add structural integrity that would be an eye sore for a land based wind farm.

Another area of potentially profitable exploitation of DAWTs is in building top applications. This is, again, due to the fact that there are

fewer obstructions and therefore less hub height is required to capture optimal wind flows. With the enhancements in performance made in this thesis, the DAWT may be one step closer to successful commercialization.

## 1.3. Overview

The thesis is broken up into several chapters that contribute to different aspects of the study. Chapter 2 discusses the theoretical background of wind energy capture and DAWTs. It then goes on to discuss some of the theory behind and reasons for adding a diffuser to the wind turbine. Chapter 3 reviews previously published research and analysis. This chapter looks at several prominent studies in the history and development of the diffuser augmented wind turbine. Chapter 4 discusses the methods used in the research that was completed in preparation for this thesis. It describes the parameters examined and outputs collected in the various stages of the study. Chapter 5 reviews the results of the research described in Chapter 4. It presents a series of relationships between geometry parameters and power augmentation. Chapter 6 summarizes the findings in Chapter 5. It goes on to draw conclusions about the diffuser augmented wind turbine based on these findings. The most significant of the findings is successfully exceeding the Betz limit based on diffuser exit area. The appendices present detailed information that supports the finding discussed in the thesis. The appendices include the presentation of a turbulence model comparison study and CFD analysis of rotor disc theory and prior designs.

## 1.4. Figures

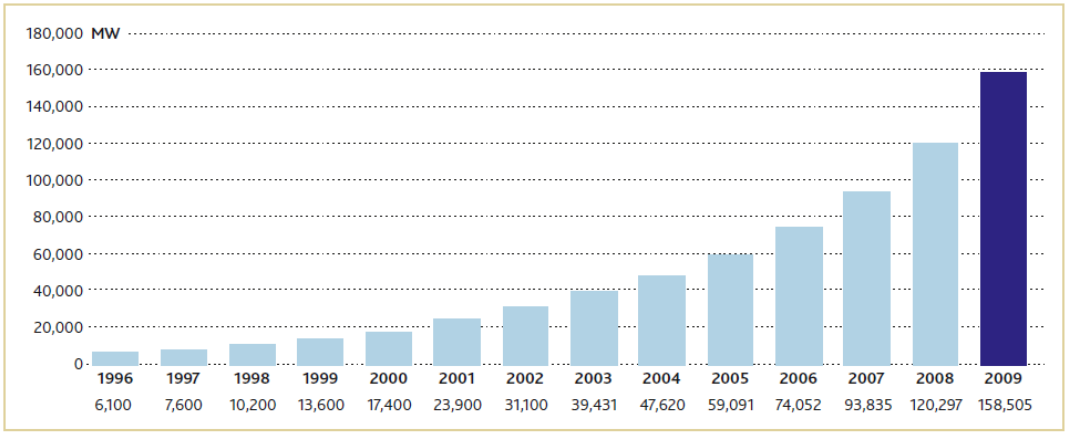


**Figure 1.1: Global Installed Wind Power Capacity from 1996 to 2009 [1]**

# CHAPTER 2: THEORY

## 2.1. Theoretical Framework for Wind Turbines

Wind energy is collected by removing kinetic energy from passing wind. This energy is turned into rotation when the wind produces a torque on the turbine blades. The rotation is usually passed through a gearbox to turn at the correct speed to operate a generator and produce a current. The energy available from wind is given by

$$P_w = \frac{1}{2}\rho U_\infty^3 A_d \tag{2.1}$$

The mass of air passing through the rotor plane or disc can be thought of a separate from the surrounding air. In this way air flowing through a traditional horizontal axis wind turbine can be considered to be a stream-tube [5]. Due to the conservation of mass and the decrease in velocity as the air approaches and passes through the rotor disc, the disc area must change with changing velocity. For conservation of mass to hold

$$\rho A_\infty U_\infty = \rho A_d U_d = \rho A_w U_w \tag{2.2}$$

The velocity slows as it approaches the turbine due to the increased pressure near the obstruction of the rotor and the absorption of kinetic energy by the rotor. In order for mass to be conserved, this slowing causes the area of the stream-tube to increase as it approaches and passes through the wind turbine. This means that the kinetic energy of the air passing through the turbine is more diffuse than it is in the free stream.

With some derivation it can be shown that the actual energy available to an ideal traditional HAWT is actually much less than the total energy contained in a given cross-section of wind. The power coefficient, $C_P$, is defined as:

$$C_P = \frac{P_W}{\frac{1}{2}\rho U_\infty^3 A_d} = 4a(1-a)^2 \quad (2.3)$$

Where $a$ is the axial flow induction factor and is defined as

$$a = \frac{U_\infty - U_d}{U_\infty} \quad (2.4)$$

Based on Equation 2.3, the maximum value for $C_p$ occurs when $a$ is equal to 1/3 and is called the Betz limit.

$$C_{P_{max}} = 16/27 \quad (2.5)$$

What this means is the energy that can be removed from the wind using a bare turbine is limited to 16/27, or 59.3%, of the total available energy. There are other real-world phenomena that further reduce the level of energy capture. Some of these sources are frictional losses and energy conversion inefficiencies, but they are not the subject of this study.

## 2.2. DAWT Momentum Theory

Based on one-dimensional momentum theory, the velocity relations within the diffuser are based primarily on the diffuser shape. In theory the location of the turbine in the diffuser does not matter. The optimal location in practice, however, is the nozzle or narrowest section of the

diffuser to minimize rotor size [6]. When examining a standard HAWT, the optimal wake pressure coefficient, $c_{p,w}$, is -0.33.

$$c_{p,w} = \frac{p_w - p_\infty}{\frac{1}{2}\rho U_\infty^2} \tag{2.6}$$

Van Bussel [6] theorized that if extra back pressure can be created at the exit of the diffuser, there is potential to exceed the Betz's limit based on diffuser exit area. With regards to the DAWT, $\gamma$ will represent exit back pressure ratio. It is defined as

$$\gamma = \frac{p_\infty - p_{exit}}{0.33} \tag{2.7}$$

$\beta$ represents the exit area ratio, also referred to as EAR.

$$\beta = \frac{A_{exit}}{A_d} \tag{2.8}$$

The power coefficient of the DAWT without additional backpressure at the exit is

$$C_p = 4a\beta(1-a)^2 \tag{2.9}.$$

This yields a maximum output of $\beta C_{pmax}$. If a dynamic pressure below -0.33 is achieved at the diffuser exit, $\gamma > 1$, then

$$C_p = 4a\beta\gamma(1-a)^2 \tag{2.10}.$$

If considered based on diffuser exit area

$$C_{p,exit} = 4a\gamma(1-a)^2 \tag{2.11}.$$

These formulas show that exceeding the Betz limit based on exit area is possible if the pressure coefficient at the exit of the diffuser is lower than

-0.33 and flow separation does not occur. Some theorists have stated that the limit of $C_{P,exit}$ for a DAWT may be 89% or greater [7, 8]. $C_{P,exit}$ will be referred to as the specific power coefficient,

$$C_{P,exit} = \frac{C_P}{\beta} \tag{2.12}.$$

The goal of the current study is to maximize the specific power coefficient. As previously shown this can be done by creating a low pressure zone at the exit of the diffuser. The difficulty with this task is that separation must be avoided for the theoretical results to be realized. This thesis will focus on achieving this fully attached flow.

# CHAPTER 3: REVIEW OF LITERATURE

Many studies have investigated methods and designs for augmenting wind turbine performance with a diffuser. One of the first theoretical papers on the topic was written in the 1950's and indentified the potentially beneficial results of creating a low pressure zone behind a traditional HAWT [9]. There was little interest in the idea until the 1970's oil crisis brought alternative energy to the forefront of discussions [10]. It was at this time that several separate researchers began in-depth studies of diffuser augmentation.

## 3.1. Physical Tests

Two prominent examples of the work done in the 1970's, are the Grumman Aerospace studies conducted by Foremann et al. [11, 12, 13, 14] and the University of Negev study conducted by Ozer Igra [15]. These investigations showed some promising results and were an important first step in the development of DAWTs. Igra's initial work involved wind tunnel studies of multiple small scale diffusers. Mesh screens of different solidity were used to simulate the resistance of a turbine and to examine the potential power of the diffuser with varying turbine thrust factors, $C_t$.

$$C_t = \frac{p_1 - p_2}{\frac{1}{2}\rho U_d^2} \tag{3.1}$$

Where $p_1$ is the pressure just upstream of the rotor and $p_2$ is the pressure just downstream of the rotor.

The first generation shroud was 7 rotor diameters long with an 8.5 degree diffuser angle. The resulting exit area ratio, EAR, was 3.5. Three different bell-shaped inlets were used with this first diffuser. The results of this wind tunnel testing showed impressive augmentation results of 2.5 to 3.0 times the performance of a bare wind turbine. The massive diffuser size was totally impractical from a commercial standpoint and Igra proceeded to a second generation short diffuser shroud. This second design used had a length to diameter ratio, LTDR, of 3.64, and EAR of 2.0 with a diffuser angle of 12.5 degrees. This design also incorporated 3 annular rings with gaps between them to help prevent flow separation. These rings also increased the exit area ratio to 10.0. The peak power augmentation, $C_{p,Betz}$ was 2.8 with 3 rings at a $C_t$ of 0.22 [15].

$$C_{P,Betz} = \frac{C_P}{C_{P\,max}} \tag{3.2}$$

As mentioned, around the same time, Foreman working for Grumman Aerospace was conducting research on a different version of the diffuser augmented wind turbine. This study focused on boundary layer control and minimizing diffuser size [12]. Grumman's initial theoretical analysis showed that optimization goals of large EAR, large velocity increase, and a negative exit pressure. Being that Grumman's goal was commercial

viability, they chose a moderate EAR in favor of lower cost. This study examined a single skin boundary-layer control type diffuser [14]. The boundary layer control device was various inlets between multiple diffuser extending rings. A wide variety of straight section diffusers with angles from 40 to 90 degrees were used. These diffusers had EARs from 1.28 to 4.94 [13]. Like Igra, Grumman used various mesh screens to simulate turbines with thrust factors between 0.37 and 0.94. Studies of ring slot height and overlap were conducted. In all over 150 configurations built and tested, but they all were base on the straight diffuser of a conic profile. The final product of the Grumman study was a 60 degree diffuser that has a LTDR of 0.715 and an EAR of 2.78. The peak augmentation, or $C_{p,Betz}$, of 2.3 was achieved with a rotor thrust factor of 0.55 in the baseline diffuser model [13]. Foreman concluded that the DAWT was not economically competitive with traditional HAWTs [11, 14]. This lead to a period of inactivity on the subject until some researchers from New Zealand decided to reexamine the subject.

In 1995 Vortec Energy Company bought the rights to some of Grumman's work and began an effort to commercialize the DAWT [16]. They teamed with the University of Auckland in New Zealand to develop a 7.3m prototype. In addition to this large scale prototype an extensive study that incorporated theoretical, CFD, and wind tunnel development was undertaken. This study resulted in several new findings and improved results. The end result of the study was a diffuser with a short 0.48 LTDR

and a 3.0 EAR [9]. The resulting performance augmentation with respect to the Betz limit was 1.73. Some of the conclusions Phillips arrived at were: augmentation is maximized when air flow is directed radially at the exit by having a large diffuser angle at the exit. Diffuser flaps were found to be best when of width roughly 5% of exit diameter.

It was found that a constant area section in around the rotor was unnecessary. The study made some promising steps forward in developing a passive boundary layer control system. The study also agreed with many previous researchers in finding that EARs over 3.0 would not provide an efficient increase in augmentation. While this study showed a reasonable level of augmentation in the smallest diffuser size to date it left some areas for improvement.

There was a significant discrepancy between power coefficient during wind tunnel testing using the filter turbine and full scale testing with a rotor in place. It was claimed that the reason for this discrepancy was the beneficial effect of the blade tip vortices in mixing the inner and boundary layer flows. While this effect is likely to have contributed to the difference in augmentation, the higher Reynolds number associated with the large scale tests have proved to be beneficial in other experiments [17].

### 3.2. Analytical Studies

A CFD study conducted in 1999 was the first to present results that showed the Betz limit was approachable in relationship to the diffuser exit area [18]. This study was conducted on a 10 degree slice of a cylindrical wind tunnel. The test tunnel extended 5 diffuser lengths upstream and 10 downstream. In addition it had a radius of 10 diffuser lengths. A NACA0015 airfoil shaped diffuser was used with a LTDR of 1.06 and a EAR of 1.84 [18]. The inlet velocity was prescribed such that the Reynolds number was $5 \times 10^7$. A Reynolds number this high would be represented by a 42m rotor in a 10m/s wind with an 89m long diffuser. As later discussed, in Chapter 5, higher Reynolds numbers yield significantly increased $C_P$ values.

This setup resulted in a rotor plane velocity increase of 1.83 with no rotor present. With a rotor present, the design showed $C_P$ results that reached 0.94 at a $C_t$ of 0.80. This results in a $C_{P,exit}$ of 0.514, or 87% of the Betz limit. This study is the first to show that the Betz limit is approachable based on diffuser EAR. A down side of this study is the small EAR, large LTDR, and very high Reynolds numbers. Later CFD design and analysis studies have shown higher $C_P$ values, but when $C_{P,exit}$ is examined they fell short [19, 20].

# CHAPTER 4: EXPERIMENTAL METHODS

This study consisted of parametric research that was conducted using Pro Engineer as a design tool and STAR CCM+, a commercially available CFD program used for analyzing problems from heat transfer to supersonic aircraft. The study was conducted in a multi-phase optimization methodology; focusing on and identifying critical relationships in an empirical study and comparing these back to previous literature findings.

## 4.1. Research Methodology

Since this study effort consists strictly of computer simulations, a standard test fixture was designed based on the guidance of previous CFD studies [17, 19]. The wind tunnel for this study was a cylinder that was 15 rotor diameters long and 10 rotor diameters wide. The large size was chosen to avoid having faulty data due to high levels of tunnel blockage. In fact, the large size of the test tunnel meant that the diffusers considered in this study only presented a 2-3% blockage.

Most of the designs considered were axis-symmetric in nature, and a 2-D model may seem adequate. This type of 2-D model would have saved a significant amount of computing time. If a 2-D model had been used, however, 3-D effects of vortices would be neglected. The decision to go with a 3-D study allowed the addition or study of vortex generating

devices and other variable angle slot or inlets. 3-D as the test wind tunnel is, it did not require that the entire 360 degrees be captured. A 45 degree slice of the tunnel was chosen to save on computing time, see Figure 4.1. The wedge wind tunnel was meshed using the STAR CCM+ polyhedral mesher, see Figure 4.2. The walls of the 45 degree slice of wind tunnel were modeled as slip walls or walls that impart no shear stress on the air.

## 4.2. Data Collection

In order to isolate diffuser design, rotor design and optimization are not considered in this study. Instead the rotor is represented with a porous media region. The region is assigned a predetermined resistance using an iteration based table. The pressure differential from the inlet to outlet of the porous region in conjunction with the velocity across the porous region is used to establish the potential for energy collection.

Several pieces of data were collected with each diffuser design that was analyzed. The inlet velocity for the wind tunnel was pre-defined for the testing in this study. The area-average velocity of the air at the front face of the rotor disc was monitored. Area-averaged pressure readings were taken at the front and rear face of the simulated rotor. The difference in pressures from these two planes is used to arrive at a pressure drop across the turbine. In the final phase of the study, force exerted on the shroud was recorded with varying turbine thrust factors. This information can

later be used for structural and extreme wind loading calculations. Varied rotor thrust factors, $C_t$, were tested for each diffuser configuration. The resulting pressure difference and velocity for each unique diffuser and turbine was then used to arrive at a power coefficient.

$$C_P = \frac{A_d U_d dP}{\frac{1}{2}\rho U_\infty^3 A_d} \tag{4.1}$$

The use of a range of turbine thrust factor settings allowed for the identification of an optimal turbine design for any given diffuser, see Table 4.1.

The meshed models contained from 60,000 to 100,000 cells. On average, 500 iterations of the solver were required for convergence of a stable solution for a given set of inputs. To ensure convergence, simulations were set to run to 1000 iterations per rotor thrust factor setting. This iteration buffer allowed less stable solutions to run through a series of 8 to 10 different thrust factors without a human monitor. Setting the simulation to automatically step through thrust factors allowed 8-12 hour simulations to be run overnight to avoid unnecessarily tying up the limited number of available software licenses. At the end of a simulation run, data was exported along with velocity and pressure difference plots for verification of convergence of monitored parameters.

### 4.3. Test Setup

Design geometries for diffusers were constructed using Pro Engineer Wildfire 3.0 CAD software. They were then exported as a universal .STP file that is compatible with STAR CCM+ and many other analytical tools. The geometry was then imported to STAR CCM+ as a group of connected surfaces. Each unique diffuser geometry was imported into the 45 degree wind tunnel. The various surfaces of the diffuser were then combined to form a single region, as defined in STAR CCM+. A simple Boolean subtract was then performed to subtract the portions of the air from the test wind tunnel that were intersected by the diffuser. In this way the inlet and other boundary conditions were shared between different analysis models. This also allows monitored outputs within the rotor and air continuums to be setup in a shared test setup file. The setup file also contained meshing parameters, thrust factor tables, and inlet velocities. The analysis models were divided into air and rotor volumes with the diffuser components being a represented as void in the air volume. A hybrid polyhedral meshing algorithm was used to mesh the air and rotor regions. The typical number of cells for a simulation was between 60,000 and 100,000. The simulation was setup as a 3-D stationary, steady state, ideal gas analysis. The turbulence model used was the Averaged Navier-Stokes method using K-Epsilon with realizable K two layer y+ wall treatment.

## 4.4. Testing Phases

There were three separate phases of design and analysis that were completed. The phases consisted of straight walled diffusers, curved diffusers, and diffuser optimization.

### 4.4.1. Straight Walled Diffusers

The initial phase of testing involved a basic characterization of some gross geometry parameters. In order to isolate the effects of various geometric variables it was decided to hold the EAR and LTDR constant for the first set of diffusers. As previously discussed, it was assumed that EARs over 3.0 would be difficult to eliminate boundary layer separation in. For this reason the EAR was set at 3.0 and LTDR was set at 1.0. All the diffusers used the same inlet profile. This was a single radius curve that had an 80 degree angle from diffuser center line to the opening at 1.09 times the rotor diameter. This bell shaped inlet had an area 1.2 times that of the turbine or diffuser throat. This initial inlet size was based on multiple resources [6, 9, 15]. The diffusers contained a constant cross-section area around the turbine followed by a straight walled diffuser, see Figure 4.3. The variables for this phase of the investigation were diffuser half angle, presence of slats, the presence of vortex generating tabs, and the presence of an outer skin on the diffuser. Table 4.2 summarizes the different geometry configurations analyzed.

Designs with 22.5, 30, 45, and 50 degrees were examined. In order to maintain the 1.0 LTDR, the constant area section of the diffusers varied in length. The 50 degree diffuser was of a stepped nature. The 50 degree diffuser included a 22.5 and 36 degree section.

Vane-type vortex generating tabs, similar to those used on small aircraft to delay separation and stall, were placed just upstream of flow separation sites on the inside of the diffusers. This was done in an attempt to identify any effects of the vortex mixing on boundary layer separation control and more importantly power augmentation [20]. The vortex generator pairs were of the vane-type and added in pairs as described in a paper by Logdberg et al. [21].

To look at the potentially beneficial effects of injecting high energy exterior flow into the low energy boundary layer inside the diffuser, the diffusers were broken into multiple sections in some cases. These slats that were created, with the breaking up of the diffuser into sections, were examined as a potential method for delay of separation. In addition, an outer skin was place around some diffusers to create a pressurized chamber from air was injected into the slats. Overall, these designs were simple to modify and served as a good format to setup analysis parameters and verify analysis methods.

### 4.4.2. Curved profiles

The first phase of the study allowed for some basic flow effects to be observed. The second phase of this study built off the extensive work performed by researchers for Grumman Aerospace and the University of Auckland [9, 13]. The first step was to accurately model the diffusers used in these studies and replicate their results. This proved fairly difficult as neither dimensional drawings nor clearly defined construction details were presented in the Grumman or Auckland papers. The diagrams presented in the papers were of generally poor quality and the low resolution of the diagrams made accurate measurement difficult. In any case, the geometries were modeled in Pro Engineer as accurately as possible. The size of the slats and material thickness for the various models had to be assumed. A number of similar geometries were evaluated that produced results comparable with the findings in the two studies. These designs were evaluated with the same test wind tunnel as the other diffuser designs described in this thesis. The details and results of these simulations can be found in Appendix B. To date the Grumman study has demonstrated the best specific power coefficient based on overall size of the diffuser although there have been questions about the validity of some of the results [9]. Due to the limitations of straight walled designs the diffusers in this phase the study used curved walls and slats similar to the Auckland design.

One of the major contributors to the enhanced performance of this style of diffuser is the inclusion of slats or annular gaps between the successive rings of the diffuser. These gaps in combination with a curved profile proved to significantly delay boundary layer separation; even with much larger included angles than those found in the initial phase of the study. The delay in separation is due to the high energy external flow increasing the energy of the boundary layer air. These slats have been used in airplane wings for many years and first showed up related to DAWTs in the research of Igra and Foreman in the late 1970's [13, 15]. The parameters that were examined in this phase of the study were LTDR, EAR, exit angle, ring gap, ring overlap, ring number, inlet size, multiple skins, wind speed, and scale.

LTDR was varied from the very short 0.48 of the Auckland diffuser to 0.83. This range, while much smaller than some previous studies, adequately encompassed the range of efficient and cost effective sizes. It also showed valuable trends on the optimal LTDR.

Exit area ratio was varied for this family of curved diffusers. The base EAR of 3.0 was the used for initial diffusers. Since separation was observed in all variations of the 3.0 EAR diffusers, it was decided to progressively decrease the exit area while maintaining a similar curve

profile. EARs of 3.0, 2.75, 2.5, 2.35 and 2.0 were investigated. It was expected that the power coefficient would decrease with decreased EAR. The item of interest, and the unknown, was how the specific power coefficient would change with EAR. The intention was to see if the diffuser became more efficient with decreased diameter.

The Auckland study reported that the optimal diffuser included angle was 55 degrees [9]. This may have been the case for the extremely short diffuser that was used in that study. When the LTDR was allowed to be increased, it opened up the possibility to have a smaller included angle on the diffuser. The exit angle for the diffusers used in this study phase varied from 45 to 60 degrees.

Annular gaps between sections of the diffusers were present in all of the phase two designs. The ring gap, or radial gap between each consecutive diffuser ring, was the same for each ring in a given diffuser geometry. This common gap size was varied from 0.58% to 0.83% of the rotor diameter. Ring overlap, or the linear distance that each ring over lapped the previous one, was varied as well. The ring overlap was varied from 0.25% to 2.0% of the rotor diameter. The idea being that there must be a balance between guiding and focusing the flow and reducing the flow due to viscous drag effects. Ring number was varied from 3 to 5 rings. The Auckland diffuser that the profiles for this study were based on had an outer surface or scoop that created a pressurized region that fed into the

boundary layer control slots. In this phase of the study diffuser profiles were compared with and without an outer scoop.

Wind speed and scale were varied over a practical range. Performance at wind velocities of 2, 5, 8, and 16m/s were used. For size variation, 4.6m and 30.5m diameter rotors were used. In effect the same factor was being varied for either case. The real reason for a performance change with variation in these parameters was the fact that the Reynolds number was being varied with different velocity and characteristic length parameters.

$$Re = \frac{VL}{\nu} \tag{4.2}$$

For this reason, only the velocity variation results are presented in Chapter 5. The Reynolds numbers for the simulations in phase 2 varied from $2.5 \times 10^6$ to $3.2 \times 10^7$. The higher Reynolds number flow is more turbulent and the viscous effects at boundary layer have less impact on the mainstream flow.

### 4.4.3. Optimization study

After the phase two data was collected and summarized several trends were found. Observing these trends and relationships, a phase three study was conducted in an effort to exceed the Betz limit. While it was clear that performance increase with increased Reynolds number, the rotor size for this phase was held at a modest 4.6m. In addition the wind

velocity was held at 5 m/s. With this noted, it should be clear that the $C_P$ results of this phase of testing could be improved by increasing rotor scale or wind velocity. In this optimization phase of the study the LTDR was re-assessed based on an optimal EAR identified in phase two, see Figure 4.4. This phase of the study varied the length of the diffuser to identify an optimal length and to collect the data that would be required to make informed engineering decisions about size and structure tradeoffs.

A diffuser with a 50 degree half angle exit and an EAR of 2.5 was chosen. The diffuser had an inlet area equal to 1.2 times the rotor area. The diffuser was broken up into multiple sections. The base diffuser body including the inlet section was 0.39 times the rotor diameter. The exit half angle of the base diffuser was 28 degrees. The blade tip gap at the narrowest section of the diffuser was 1.0% of the rotor diameter. The base diffuser body was followed by 4 rings. The rings got progressively shorter with larger diameter. The lengths of the rings were 10.4%, 8.8%, 7.1%, and 5.4% of the rotor diameter. Each ring increased the exit angle by another 6.5 degrees for a 50 degree angle at the exit of the final ring. The gap between each ring was 0.78% of the rotor diameter and the overlap was 0.92% of the rotor diameter. The total LTDR for the initial diffuser with rings was 0.58. Based on this rotor an investigation of LTDR, ring gap, and ring overlap was conducted.

The ring gap size and ring overlap were varied plus and minus 10% from the baseline geometry. The LTDR was varied from 0.5 to 0.78. This was varied primarily by changing the length of the base diffuser. At the extremes, the base diffuser exit angle had to be adjusted to maintain ring length and angles. The overall exit half angle of 50 degrees was maintained for all the variations. In addition no changes to the inlet side of the diffuser were made.

#### 4.4.4. Final Design

After the findings of the optimization phase of the study there was one clear choice for the optimal diffuser. The final diffuser design had an EAR of 2.52 and a LTDR of 0.72, see Figure 4.5. This diffuser was re-analyzed to capture wind force data. In addition some additional post-processing steps were conducted to compare the results back to theoretical works on the topic of DAWTs. This diffuser was also used for a turbulence model sensitivity study, Appendix A.

## 4.5. Figures

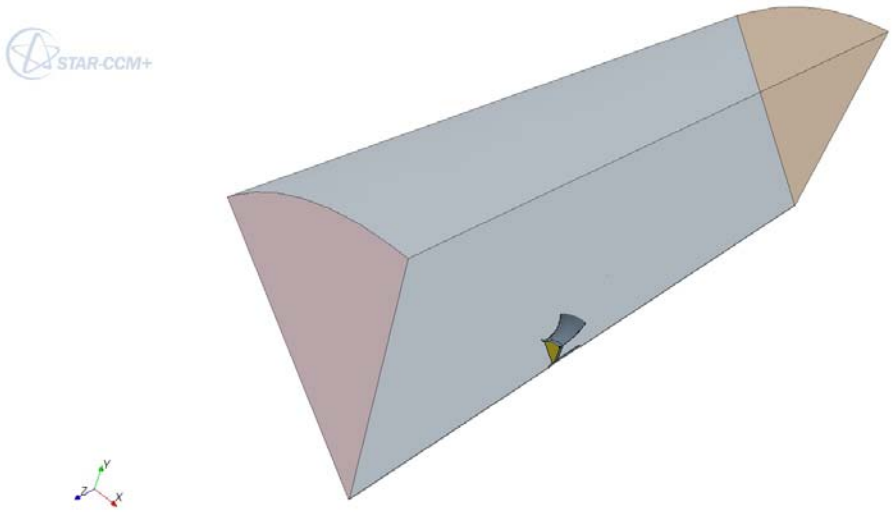

**Figure 4.1: Screenshot of the 45 degree Test Wind Tunnel in STAR CCM+**

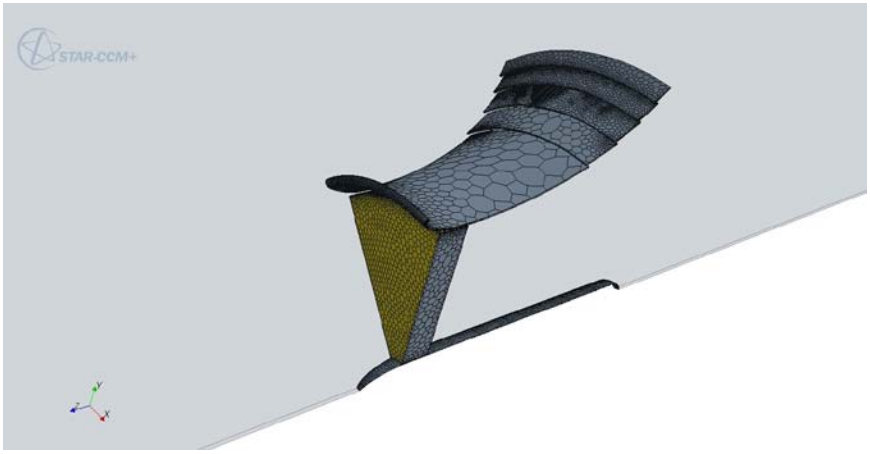

**Figure 4.2: Screenshot of Meshed Surface of a Diffuser and Rotor Model in STAR CCM+**

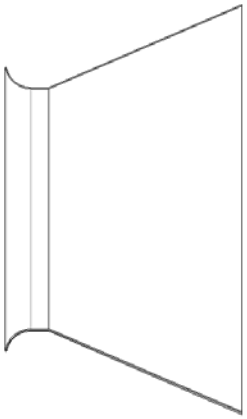

**Figure 4.3: 22.5 degree Diffuser from Phase One Testing**

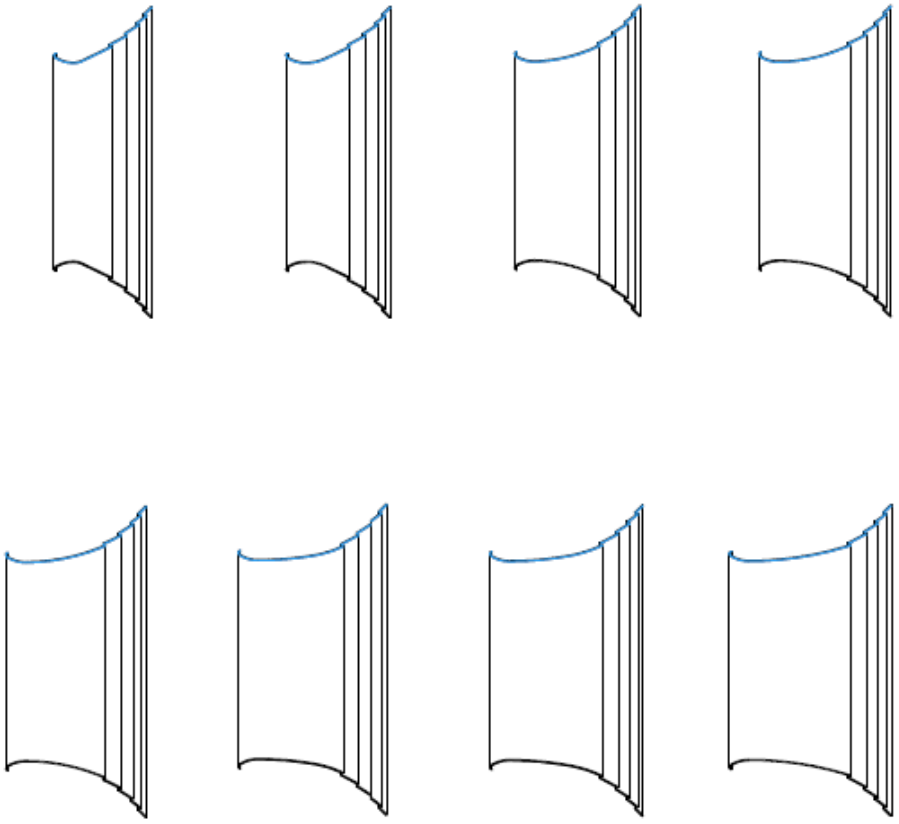

**Figure 4.4: Diffuser Profiles used in Optimization Phase LTDR Study**

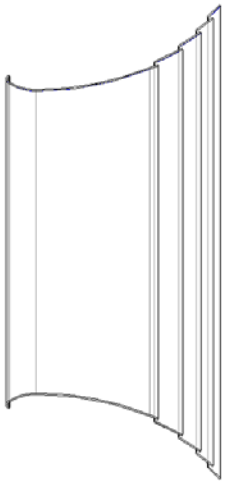

**Figure 4.5: Profile of the Best Performing Diffuser from Phase Three Testing**

## 4.6. Tables

**Table 4.1: Thrust Coefficients with Respective Rotor Model Parameters Assigned to CFD Filter Elements**

| Ct | dP/L |
|---|---|
| 0.300 | 0.472 |
| 0.350 | 0.551 |
| 0.400 | 0.630 |
| 0.450 | 0.709 |
| 0.500 | 0.787 |
| 0.550 | 0.866 |
| 0.650 | 1.024 |
| 0.700 | 1.102 |
| 0.750 | 1.181 |

**Table 4.2: Phase One Parameter Variation Table**

| Run | Half Angle | Vortex Generators | Slats | Skins |
|---|---|---|---|---|
| 1111 | 30 | N | N | 1 |
| 1112 | 30 | Y | N | 1 |
| 1121 | 30 | N | Y | 1 |
| 1221 | 30 | N | Y | 2 |
| 2111 | 22.5 | N | N | 1 |
| 3111 | 45 | N | N | 1 |
| 4111 | 50 stepped | N | N | 1 |
| 4121 | 50 stepped | N | Y | 1 |
| 4221 | 50 stepped | N | Y | 2 |

# CHAPTER 5: RESULTS AND DISCUSSION

## 5.1. Data Reduction

Each diffuser test was run for 1,000 iterations at each rotor thrust factor. The resulting data set consisted 10,000 data points that summarized dP, Velocity, and various residuals. In order to get meaningful and comparable information from these values, a data point well after solution stabilization was chosen. The sample value was typically taken after 950 iterations despite the fact that stabilization occurred earlier in most cases. The comparable output was $C_p$.

## 5.2. Straight Walled Diffusers

The first phase of the study yielded very dismal results, see Table 5.1. Admittedly, this phase of the study more of a familiarization exercise and was not really intended to perform well. All of the straight walled diffusers showed some degree of separation of the flow from the inner edge of the shroud. The best performer was the 22.5 degree diffuser, which only showed separation on the final 30% of the inner surface of the diffuser. This was expected, as the recommended maximum angle to avoid separation in a sub-atmospheric environment is 8-10 degrees [15]. The 45 degree diffuser showed a massive separation and recirculation zone in the downwind region which reduced the mass flow of air through

the diffuser. The highest level of $C_p$ was only 1.19, see Figure 5.1. The peak $C_p$ was found with $C_t$ of the rotor set at 0.75.

The placement of tabs on various locations along the inner surface of the diffuser and outer surface of the hub was evaluated. The best performing location proved to be placing the vortex generating tabs on the inner surface of the diffuser just upstream the point of boundary layer separation. The vortex generators resulted in increased mixing of the high energy inner flow and lower energy boundary layer. In this case, however, the gross effect was the reduction of the mass flow through the diffuser despite delayed separation, see Figure 5.2. It appears that the additional drag from the vortex generators overpowered the beneficial effects of the boundary layer mixing and can be attributed for this reduction in power output. With this discovery, the vortex generator tab design parameter was ruled out for the future phases of the study.

The addition of annular gaps or slats in the diffuser was investigated. The gaps did not provide the boundary layer control that was expected based on previous works. In this case, the addition of gaps resulted in a clear decrease in power output, see Figure 5.3. This is thought to be the result of non-optimal gap and overlap parameters. In addition to the slats, the addition of an outer skin was evaluated. The addition of an outer skin showed a modest increase in power output, see figure 5.4.

As the initial intention of this study was to build a prototype diffuser and test it in a wind tunnel, these phase one diffusers were designed for a rotor only 0.35m in diameter. At this small scale the viscous effects of air play a much larger role on performance than they would on a more real-world sized diffuser. The low Reynolds number air flow showed significantly lower performance than later simulations that were conducted. A larger version of the 22.5 degree diffuser was analyzed for a comparison of results between these small wind tunnel-scaled models and a larger scale private use or utility scale model. This larger model showed a 25.2% improvement in $C_P$. Later stages of testing were conducted on a diffusers designed for a 4.6m diameter rotor. This larger size, while still not equal, showed results that were more comparable with industrial sized rotors.

### 5.3. Curved Geometry Study

As mentioned this phase of the study moved to a 4.6m rotor diameter. The general geometries were of a curved nature roughly based off of extended versions of the Auckland diffuser study [9]. A summary of the results can be found in Table 5.2.

### 5.3.1. Length to Diameter Ratio

LTDR showed a very significant contribution to the $C_P$ of the diffuser, see Figure 5.5. The shorter diffusers showed high levels of separation at the rear-most portion of the diffuser. The shorter diffusers also produced a wider peak $C_P$. This is probably due to the fact that as separation occurred any potentially peak performance region was reduced resulting in a broader $C_P$ versus $C_t$ curve with a lower peak. The longer diffusers showed a significant peak in the lower $C_t$ zone from 0.25 to 0.35. The longer the diffuser, the higher and more narrow banded this peak zone became. This phase of the study showed a roughly linear relationship between LTDR and $C_p$. Since there were still signs of separation at the longest LTDR in this study, the range should have been extended to expose the relationship in a fully attached flow. This was noted and addressed in the later optimization phase of the study.

### 5.3.2. Exit Area Ratio

Exit area played a very large role in the power coefficient. While this result was expected, there were other interesting findings that resulted. The $C_P$ increased with increasing EAR. The relationship between these values did not show a linear increase, it resulted in a curve with diminishing returns as the EAR increased, see Figure 5.6. This indicated that perhaps the more appropriate value to look at would be $C_{P,exit}$ as EAR was varied, see Figure 5.7. Plotting these two values against each other resulted in a clear break point and a potentially optimal value. As the

EAR decreased from 3.0 to 2.5, $C_{P,exit}$ increased from 0.55 to 0.61. This was a 10 % increase in efficiency of the diffuser. More importantly this reduction in EAR from the originally selected value resulted in a diffuser that was giving a value of power coefficient higher than the Betz limit for its given shroud diameter. This is the first diffuser to yield results that exceed the Betz limit when compared to diffuser diameter.

### 5.3.3. Exit Angle

Exit Angle results showed that an important balance must be met. On one hand, larger diffuser exit angles have to potential to create a wider low pressure wake downwind of the diffuser. However, the larger diffuser angles in this study resulted in separation of the interior flow from the inner surface of the diffuser. This separation caused a recirculation zone which caused a collapse of the potentially large low pressure wake from the large included angle. In this study a 45 to 50 degree diffuser performed marginally better, 1.6%, than the 55 and 60 degree diffusers, see Figure 5.8.

### 5.3.4. Wind Velocity and Rotor Scale

Varying the wind speed and scale of the diffuser had the same basic effects on the fluid dynamics of the analysis. Both varied the Reynolds number. From the results in this study, increased Reynolds numbers led to increased $C_P$ due to a reduction in shear forces imparted on the air flow.

The wind speed was varied from 2m/s to 16 m/s. The resulting range of Reynolds numbers ranged from 2.5 x $10^6$ to 3.2 x $10^7$. Over this range, the power coefficient showed a 3.5% increase from the lowest to highest wind speeds, see Figure 5.9. The scaling effects were not explored in more depth since the general trend was established by varying the velocity.

### 5.3.5. Ring Gap, Ring Overlap, Ring Number, and Inlet Size

Each of these parameters appeared to each show an optimal zone. While the effects of being slightly off of the optimal values may have been small, without the study of these factors a performance change of over 10% may have been overlooked. Varying the inlet diameter by plus and minus 10% only resulted in a 2.8% variation in the observed $C_P$, see Figure 5.10. This agrees with some previous works that stated inlet ratio optimization was not as critical as other geometry effects in producing enhanced power [6]. The same relationship was found with the ring gap. Ring gap was varied in 0.08% of the rotor diameter increments from 0.58% to 0.83% of the rotor diameter while the ring overlap was held constant at 1.25% of the rotor diameter. $C_P$ levels varied by 5.1% for a ring gap variation over the range mentioned, see Figure 5.11. The optimal value was found to be 0.78% of the rotor diameter. Ring overlap was varied from 0.25% to 2.0% of the rotor diameter while the ring gap was held at 0.75% of the rotor diameter. The resulting peak $C_P$ levels varied by 4.6%, see Figure 5.12. The optimal value of ring overlap was 0.92% of the rotor diameter. The addition of an

outer shell resulted in a decreased level of augmentation for the cases examine in this phase, see Figure 5.13.

## 5.4. Final Design Optimization Phase

### 5.4.1. LTDR Re-examined

Based on the $C_P$ versus EAR finding in the previous section a smaller 2.52 EAR diffuser was used to re-examine the LTDR relationship over a wider range of values, see Table 5.3. This phase revealed a different relationship. $C_P$ versus LTDR showed an asymptotic relationship. Once fully attached flow was attained, roughly around a 0.7 LTDR, the performance gains quickly leveled off, see Figure 5.14. The longer diffusers also displayed a more narrow range of peak values similar to the findings in the phase two study, see Figure 5.15. It is expected that as the LTDR continued to increase there would be a reduction in augmentation brought on by internal drag effects on the lengthy inner surface of the diffuser. This may explain why some of Igra's early designs with extreme LTDRs performed more poorly than expected. The optimal LTDR most certainly involves multiple variables including the EAR and additional injected mass flow levels. It can be summed up, that as soon as an LTDR is achieved that allows for minimal separation of flow for a given EAR and supplemental mass flows, the returns of increased diffuser length quickly diminish. In addition more length means more cost for construction and more weight for support structure. The intention of this

phase of the study was to look at LTDR over a practical range to aid in the later selection of design tradeoffs.

### 5.4.2. Final Diffuser Design

The final diffuser design had an EAR of 2.52 and a LTDR of 0.72. The design exceeded the Betz limit by 4.0% based on the area of the diffuser with a $C_P$ of 1.554 and $C_{P,exit}$ of 0.613, see Table 5.3. This figure was for a rotor diameter of only 4.6m and a wind speed of just 5m/s. As discussed in the study, with higher Reynolds number, comes more turbulent flow reduced drag losses and higher values of power augmentation. Figure 5.16 shows the large sub-atmospheric pressure region in the wake of the diffuser. The diffuser show a fairly wide peak performance region, see Figure 5.17. It showed similar values of $C_P$ over a range of $C_t$ from 0.30 to 0.45. When $C_P$ was plotted against $C_{t,amb}$ the results showed a peak very close to $C_{t,amb} = 1$, see Figure 5.18. This is the optimal $C_{t,amb}$ value predicted by Van Bussel [6]. An interesting finding is that the force exerted on the diffuser by the wind is directly proportional to $C_P$, see Figure 5.19. This final diffuser also showed minimal signs of separation, see Figure 5.20.

## 5.5. Discussion

Exceeding the Betz limit based on EAR has been achieved in this CFD study. However, the real world costs and compromises that the 1970's Grumman study focused on in great detail still exist [14]. These factors include costs related to: diffuser material and construction, support

structure, and extreme wind loading. The fact that this study has demonstrated the ability to exceed the Betz limit with an actual design and detailed CFD analysis is a significant step in wind power research. Up to this point only theoretical studies have shown that this task was possible. The fact remains that the added structural requirements and material costs associated the DAWT make it significantly more costly per kWhr than a traditional wind turbine.

## 5.6. Figures

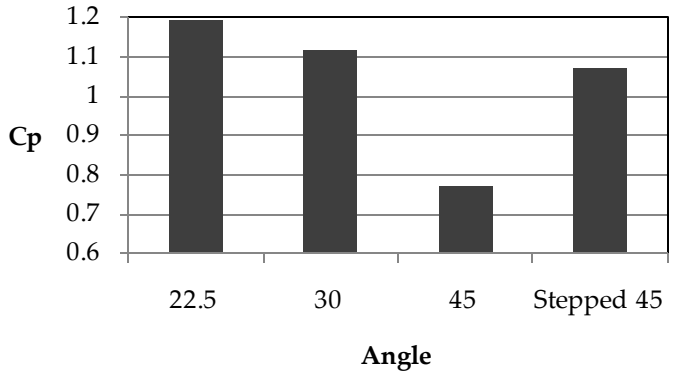


**Figure 5.1: Variation of Power Coefficient, $C_P$, with Exit Angle in Phase One Diffusers**

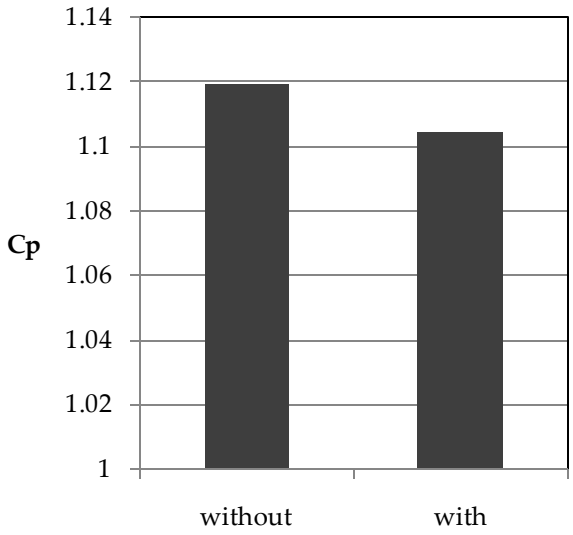


**Figure 5.2: Variation of Power Coefficient, $C_P$, with Addition of Vortex Generator Tabs in Phase One Diffusers**

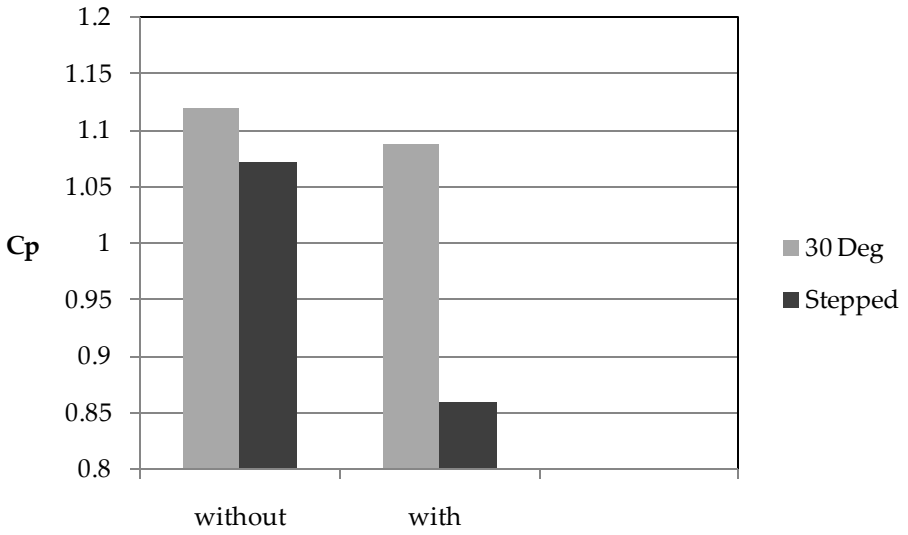


**Figure 5.3: Variation of Power Coefficient, $C_P$, with Presence of Gaps in Phase One Diffusers**

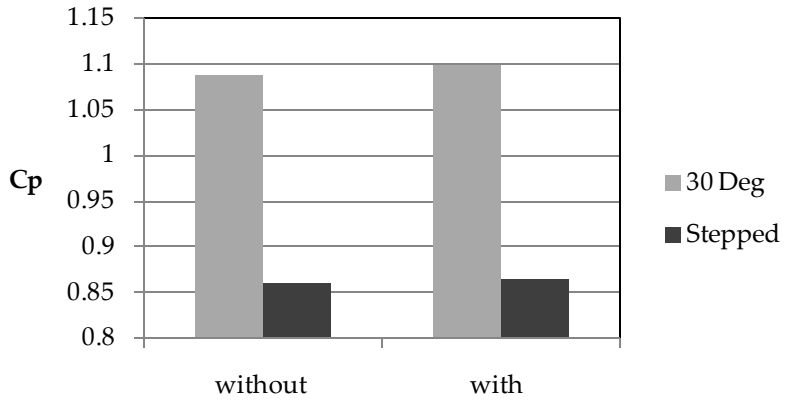


**Figure 5.4: Variation of Power Coefficient $C_P$, with the Presence of an Outer Skin in Phase One Diffusers**

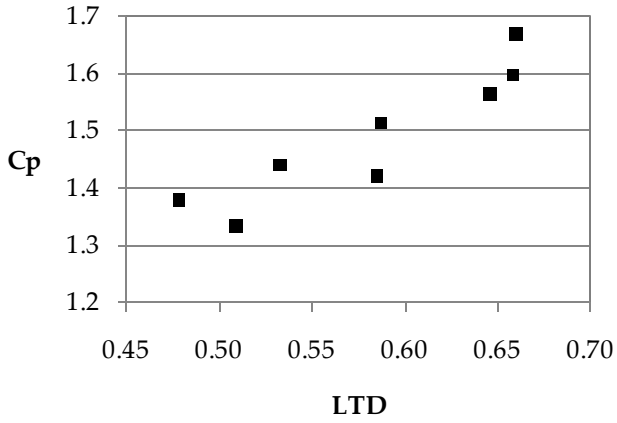


**Figure 5.5: Variation of Power Coefficient, $C_p$, with Length to Diameter Ratio in Phase Two Diffusers**

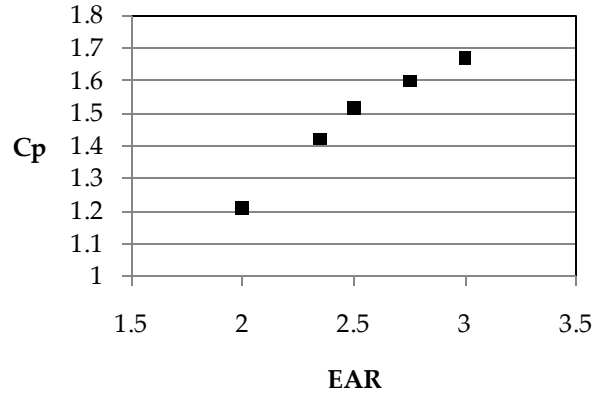


**Figure 5.6: Variation of Power Coefficient, $C_p$, with Exit Area Ratio in Phase Two Diffusers**

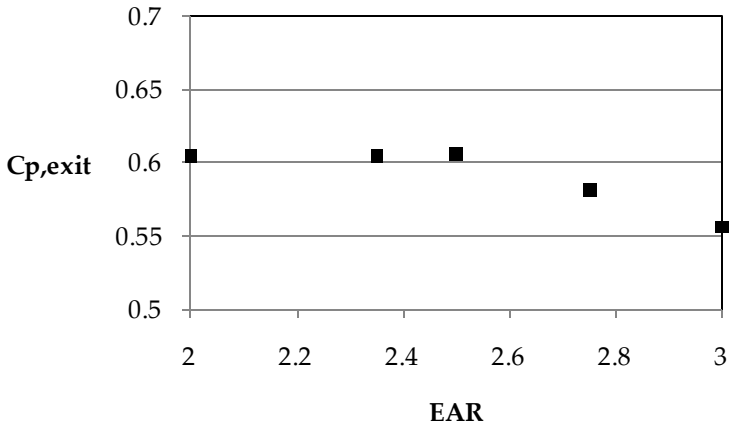


**Figure 5.7: Variation of Specific Power Coefficient, $C_{p,exit}$, with Exit Area Ratio in Phase Two Diffusers**

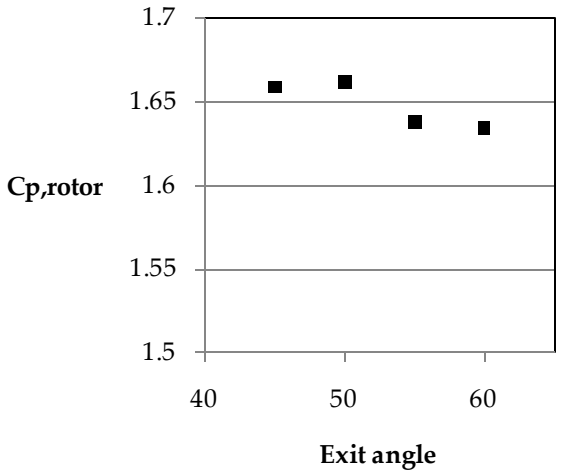


**Figure 5.8: Variation of Power Coefficient, $C_p$, with Exit angle in Phase Two Diffusers**

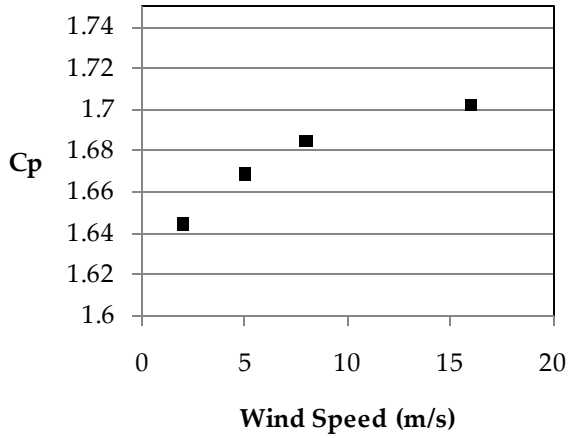


**Figure 5.9: Variation of Power Coefficient, $C_p$, with Wind speed in Phase Two Diffusers**

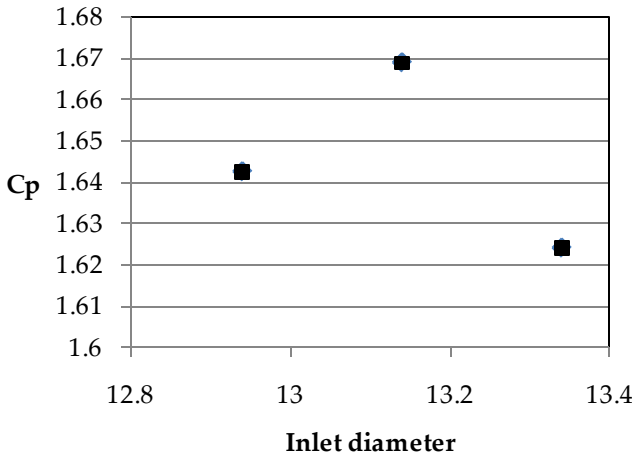


**Figure 5.10: Variation of Power Coefficient, $C_p$, with Inlet Diameter in Phase Two Diffusers**

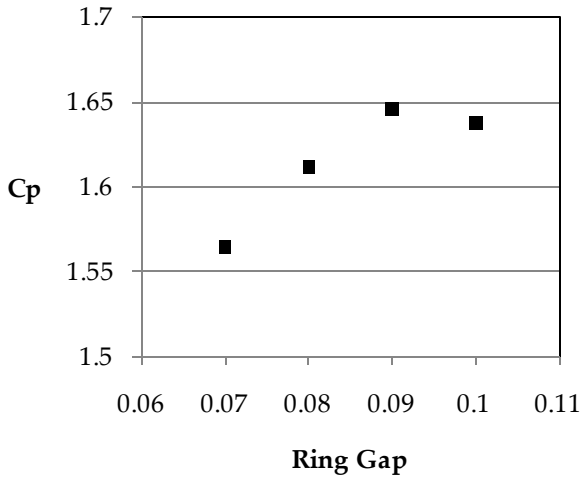


**Figure 5.11: Variation of Power Coefficient, $C_p$, with Ring Gap Size in Phase Two Diffusers**

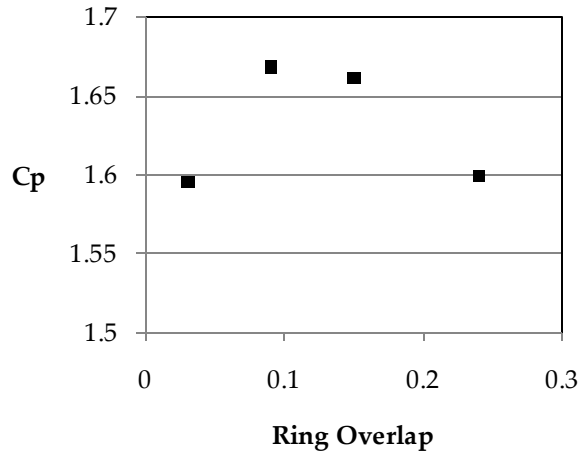


**Figure 5.12: Variation of Power Coefficient, $C_p$, with Ring Overlap Distance in Phase Two Diffusers**

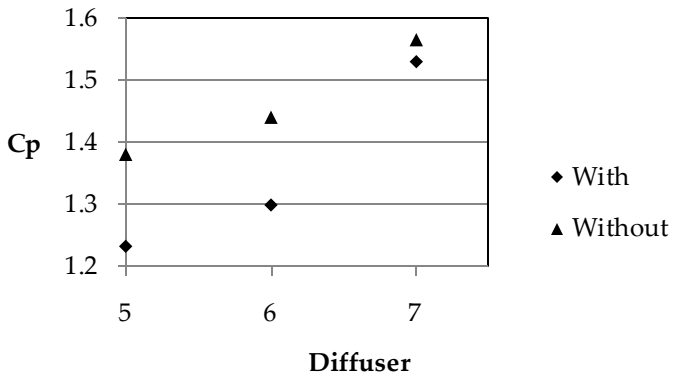


**Figure 5.13: Variation of Power Coefficient, $C_P$, with Presence of an Outer Shell in Phase Two Diffusers**

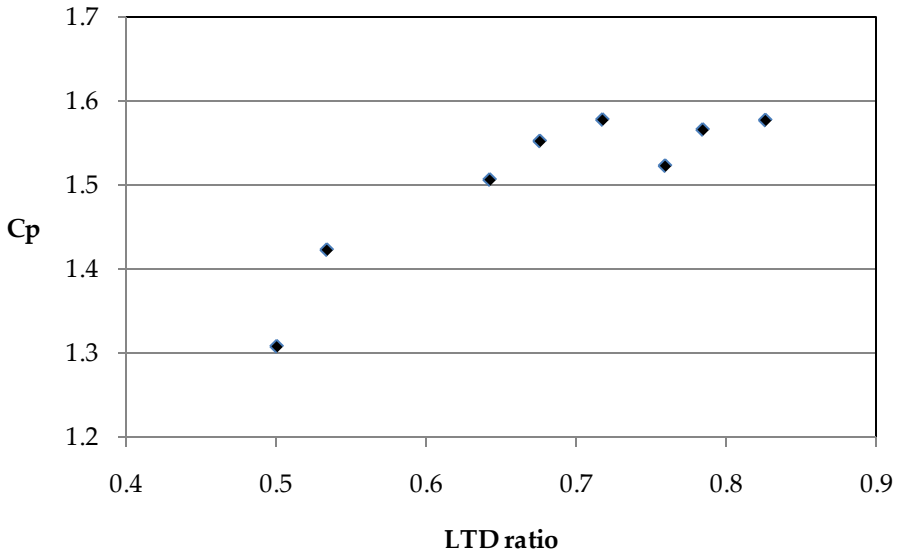


**Figure 5.14: Variation of Power Coefficient, $C_P$, with Length to Diameter Ratio in Phase Three Diffusers**

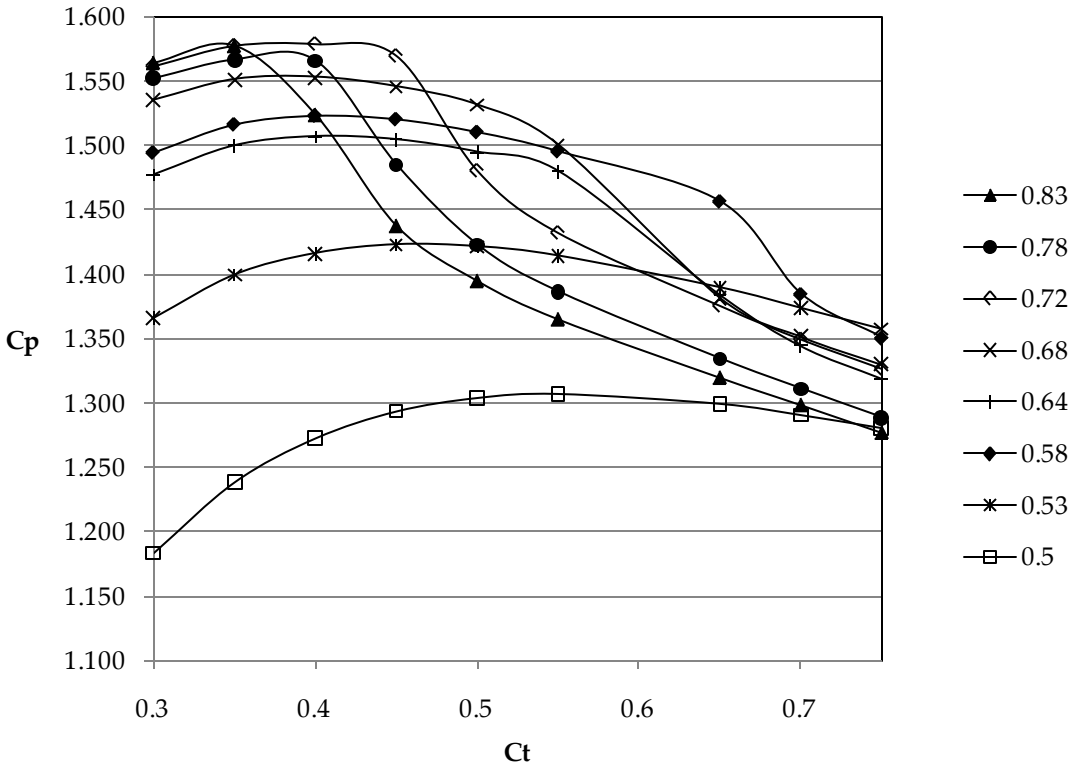


**Figure 5.15: Variation of Power Coefficient, $C_p$, with Local Thrust Coefficient in Phase Three Diffusers**

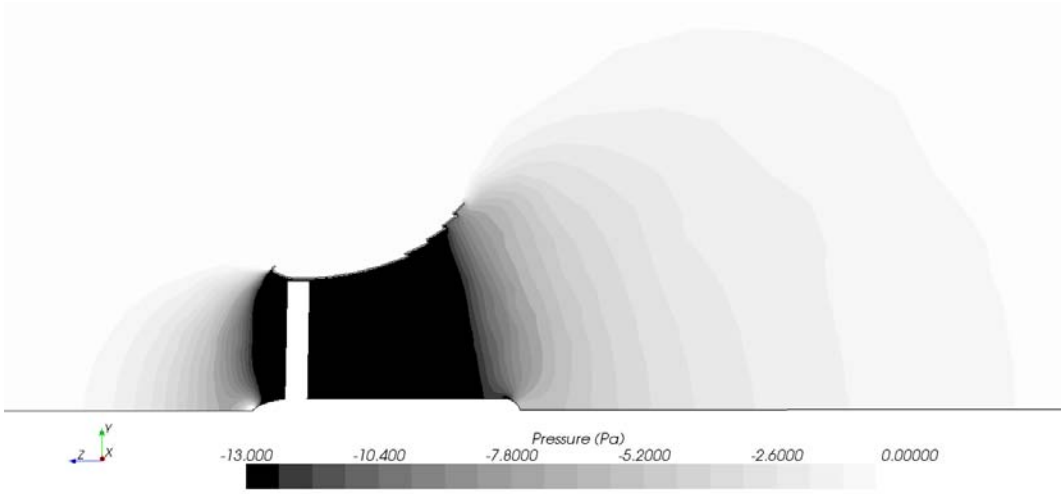


**Figure 5.16: Pressure Gradient of Final Diffuser Demonstrating a Sub-atmospheric Pressure in a Large Wake Zone**

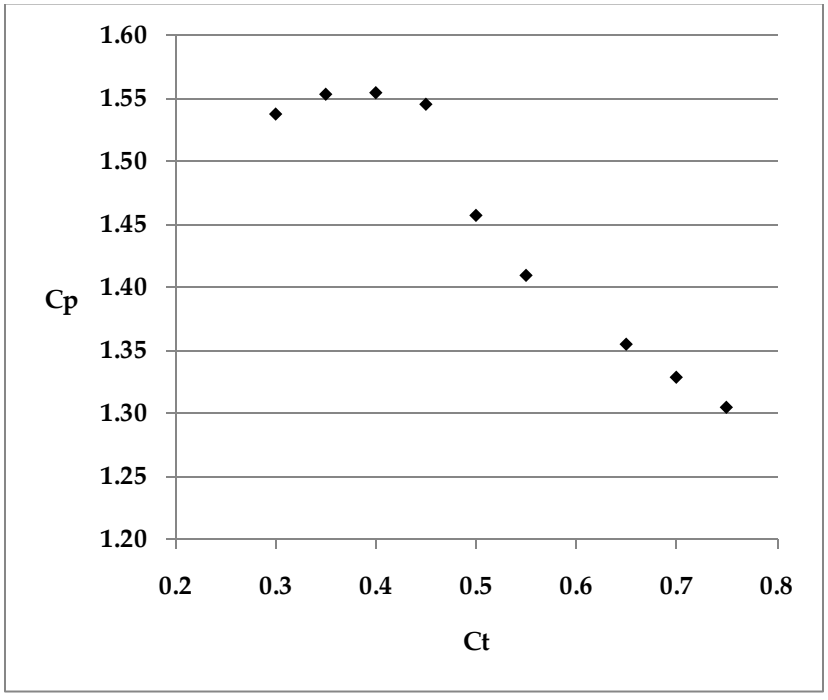


**Figure 5.17: Variation of Power Coefficient with Local Thrust Coefficient for Final Diffuser Demonstrating a Peak Value Near 0.38.**

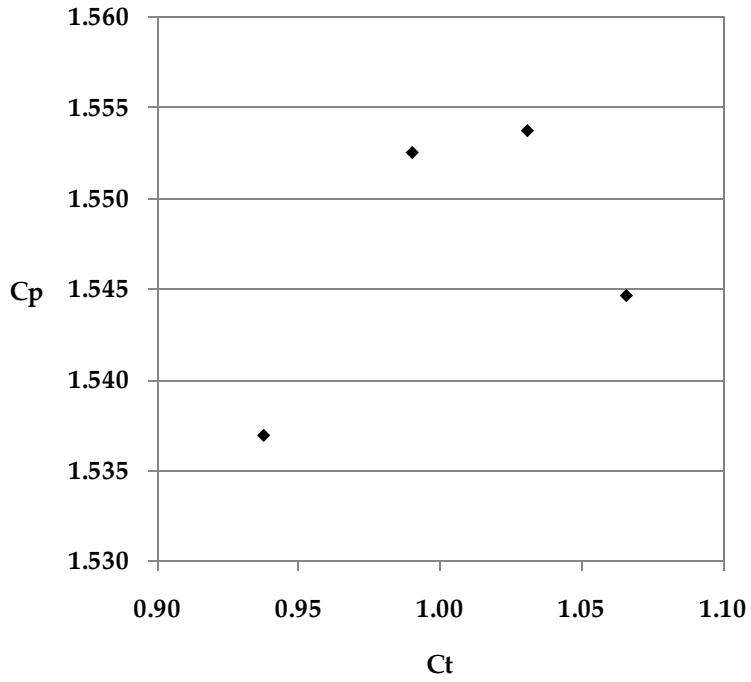


**Figure 5.18: Variation of Power Coefficient with Ambient Thrust Coefficient for Final Diffuser Demonstrating a Peak Value Near 1.0**

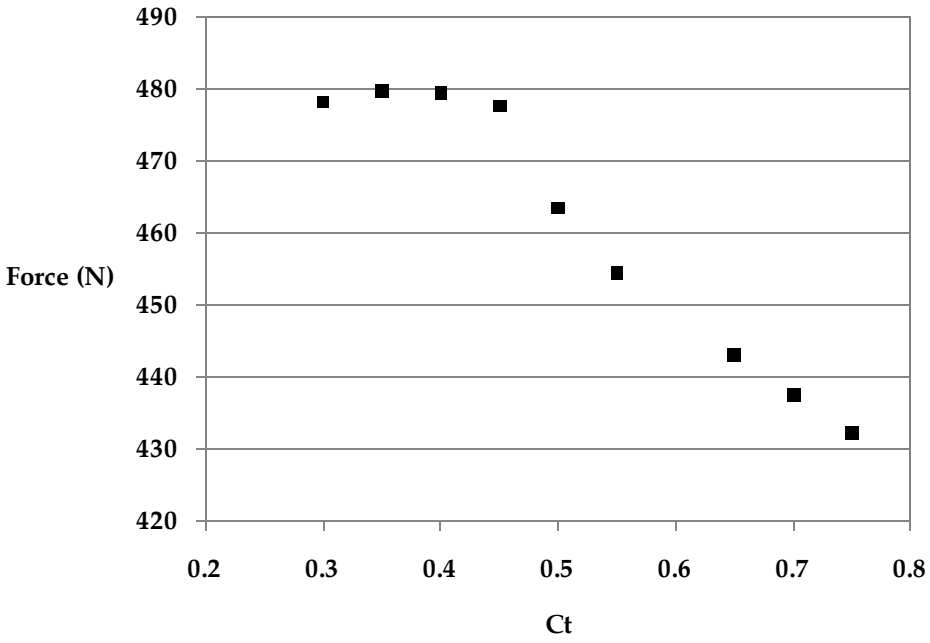


**Figure 5.19: Variation of Force with Local Thrust coefficient**

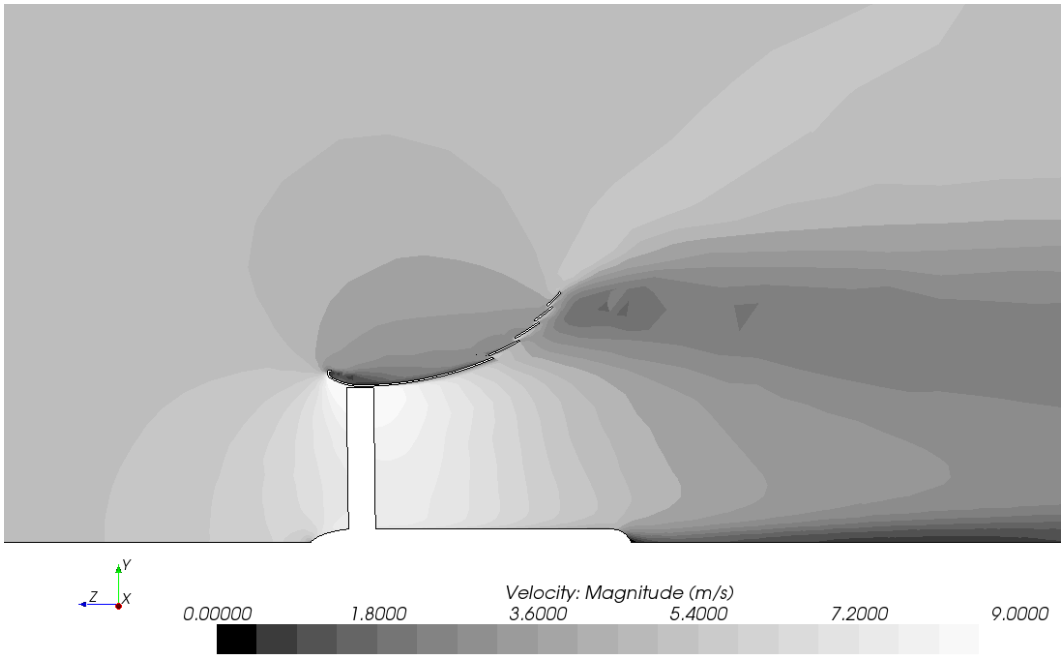


**Figure 5.20: Velocity Gradient of Final Diffuser Showing Minimal Signs of Separation at the Rear Edge of the Diffuser**

## 5.7. Tables

**Table 5.1: Phase 1 Design Parameters and Results**

| Run | Cp | Half Angle | Vortex Generators | Slats | Skins |
|---|---|---|---|---|---|
| 1111 | 1.119 | 30 | N | N | 1 |
| 1112 | 1.105 | 30 | Y | N | 1 |
| 1121 | 1.089 | 30 | N | Y | 1 |
| 1221 | 1.100 | 30 | N | Y | 2 |
| 2111 | 1.191 | 22.5 | N | N | 1 |
| 3111 | 0.772 | 45 | N | N | 1 |
| 4111 | 1.071 | 50 stepped | N | N | 1 |
| 4121 | 0.860 | 50 stepped | N | Y | 1 |
| 4221 | 0.865 | 50 stepped | N | Y | 2 |

**Table 5.2: Phase 2 Design Parameters and Performance Summary**

| Profile | $C_p$ | $C_t$ at Peak $C_p$ | EAR | LTDR | $C_P/C_{P,exit}$ |
|---|---|---|---|---|---|
| 6 | 1.440 | 0.55 | 3.00 | 0.533 | 2.429 |
| 6.2 | 1.299 | 0.60 | 3.00 | 0.533 | 2.190 |
| 8 | 1.565 | 0.50 | 3.00 | 0.646 | 2.639 |
| 8.2 | 1.529 | 0.42 | 3.00 | 0.646 | 2.579 |
| 9 | 1.612 | 0.42 | 3.00 | 0.648 | 2.718 |
| 10 | 1.646 | 0.40 | 3.00 | 0.640 | 2.775 |
| 11 | 1.638 | 0.40 | 3.00 | 0.636 | 2.762 |
| 12 | 1.634 | 0.45 | 3.00 | 0.617 | 2.756 |
| 13 | 1.662 | 0.40 | 3.00 | 0.659 | 2.802 |
| 13.5 | 1.596 | 0.40 | 2.75 | 0.631 | 2.692 |
| 14 | 1.642 | 0.35 | 3.00 | 0.640 | 2.770 |
| 15 | 1.659 | 0.40 | 3.00 | 0.672 | 2.798 |
| 16 | 1.599 | 0.40 | 3.00 | 0.651 | 2.697 |
| 17 | 1.669 | 0.40 | 3.00 | 0.659 | 2.814 |
| 17.2 | 1.598 | 0.40 | 2.75 | 0.658 | 2.695 |
| 17.4 | 1.514 | 0.40 | 2.50 | 0.587 | 2.553 |
| 17.6 | 1.422 | 0.45 | 2.35 | 0.585 | 2.398 |
| 17.8 | 1.209 | 0.50 | 2.00 | 0.532 | 2.039 |
| 18 | 1.595 | 0.45 | 3.00 | 0.662 | 2.690 |
| 19 | 1.624 | 0.45 | 3.00 | 0.658 | 2.739 |
| 20 | 1.611 | 0.45 | 3.00 | 0.654 | 2.716 |
| 21 | 1.333 | 0.55 | 3.00 | 0.509 | 2.249 |

**Table 5.3: Phase 3 Design Parameters and Performance Summary**

| Design | EAR | LTDR | $C_p$ | $C_{p,exit}$ | $C_{p,exit}/C_{Pmax}$ |
|---|---|---|---|---|---|
| 1 | 2.52 | 0.583 | 1.475 | 0.58524 | 0.988 |
| 2 | 2.52 | 0.783 | 1.541 | 0.61168 | 1.032 |
| 3 | 2.52 | 0.825 | 1.553 | 0.6161 | 1.040 |
| 4 | 2.52 | 0.642 | 1.483 | 0.58833 | 0.993 |
| 5 | 2.52 | 0.500 | 1.287 | 0.51053 | 0.862 |
| 6 | 2.52 | 0.717 | 1.553 | 0.61633 | 1.040 |
| 7 | 2.52 | 0.675 | 1.528 | 0.60634 | 1.023 |
| 8 | 2.52 | 0.533 | 1.400 | 0.55559 | 0.938 |

**Table 5.4: Final Diffuser Design Performance Summary**

| EAR 2.52 LTDR 0.72 | Value |
|---|---|
| Velocity Speed up | 1.530 |
| Exit Pressure Coefficient | -0.830 |
| Ambient thrust Coefficient | 1.030 |
| $C_p$ | 1.554 |
| $C_{p,exit}$ | 0.613 |

# CHAPTER 6: CONCLUSION

The increase in computing power and the proliferation of CFD software has made it possible to reassess the work of previous researchers without the massive funding that was necessary to fund the original studies. The days of going straight from the drawing board to a test lab are long gone. The idea of augmenting wind power collection devices has been around since wind power collection itself. The diffuser augmented wind turbine in its present sense has been developed over the last 50 years. During this time there have been numerous studies funded by governments and large companies. Most of these studies made an effort to understand important geometry parameters and there effects on power augmentation. Studies like those conducted by Grumman and Auckland made compromises for cost effectiveness too early in their work to fully explore the limits of the diffuser augmented wind turbine. By initially restricting the diffuser LTDR they effectively put a limit on how efficient the diffusers they test could be.

This thesis set out to find if, as momentum theory predicts, the diffuser augmented wind turbine can exceed the Betz limit based on its exit area. To that question the answer has been presented; yes. The final diffuser design had an EAR of 2.52 and a LTDR of 0.72. The final design that was analyzed in this study exceeded the Betz limit by 4.0% based on the area of the diffuser with a $C_p$ of 1.554 and a $C_{P,Betz}$ of 2.62. This figure was for a

rotor diameter of only 4.6m and a wind speed of 5m/s. As discussed in the study, with higher Reynolds number, comes more turbulent flow, reduced drag losses, and higher values of $C_p$. The figures in this study are based on area averaged velocity and pressure outputs which proved to be more conservative and consistent than the pressure and velocity readings taken at diffuser mounted pressure ports and single point anemometers. This study did also not include rotor tip vortex generation or wake rotation and the beneficial effects they had on separation delay in the boundary layer and resulting increased augmentation [22]. When testing with a rotor in place it is expected that the available power based on pressure readings will be higher than the CFD results because of these phenomena.

## 6.1. Recommended Future Studies

The next step for this design is to verify the findings of this thesis with wind tunnel testing. For a comparison with results in the CFD study, initial testing should be performed with the wind turbine simulated by a filter or mesh with resistance equal to the optimal $C_t$. The wind tunnel testing would need to replicate the Reynolds numbers seen in this study for a valid comparison. This could be performed using a pressurized wind tunnel, or more likely, higher wind velocity. Assuming the findings of such testing verify the results presented in this thesis, a rotor would be designed for the thrust coefficient and velocity profile of the final diffuser design.

A model should be chosen to provide a thrust coefficient near the peak efficiency of the diffuser, in the 0.35 to 0.45 range. This would be followed by wind tunnel testing. At this point it would be expected that the beneficial results of blade tip vortices on improving the potential for energy capture would result in a higher $C_p$ than found in this study. Up to this point the $C_p$ was based on pressure and velocity readings. Once the power is defined by a torque and rotational speed, instead, losses associated with a particular blade design will become a major factor in the performance of the system.

# REFERENCES


[1] Global Wind Energy Council (GWEC). GWEC Global Wind 2009 Report. [Report on the Internet]. Belgium: GWEC; 2010 [cited 2010 June 13]. [66 p]. Available from: http://www.gwec.net/fileadmin/documents/Publications/Global_Wind_2007_reprep/GWEC_Global_Wind_2009_Report_LOWRES_15th.%20Apr..pdf.

[2] Singer C, Holyward EJ, Hall AR, Williams TI. A History of Technology, Volume II: The Mediterranean Civilizations and the Middle Ages. Oxford: Clarendon Press; 1956. 846 p.

[3] Sathyajith M. Wind Energy: Fundamentals, Resource, Analysis and Economics. Netherlands: Springer; 2006. 246 p.

[4] Veers PS, Butterfield S. Extreme Load Estimation for Wind Turbines: Issues and Opportunities for Improved Practice. 2001 ASME Wind Energy Symposium. Reno, Nevada, AIAA-2001-0044; 2001. 10 p. Available from: http://windpower.sandia.gov/asme/aiaa-2001-004.pdf

[5] Burton T, Sharpe D, Jenkins N, Bossanyi E. Wind Energy Handbook. England: John Wiley & Sons, Ltd; 2001. 642 p.

[6] Van Bussel GJW. The Science of Making More Torque From Wind: Diffuser Experiments and Theory Revisited. Journal of Physics: Conference Series, IOP Publishing 2007;75:1-12. Available from: http://iopscience.iop.org/1742-6596/75/1/012010.

[7] Jamieson PM. Beating Betz: Energy Extraction Limits in a Constrained Flow Field. Journal of Solar Energy Engineering 2009;131(3). 6 p.

[8] Jamieson P. Generalized Limits for Energy Extraction in a Linear Constant Velocity Flow Field. Wind Energy 2008; 11:445–457.

[9] Phillips DG. An Investigation on Diffuser Augmented Wind Turbine Design [PhD Dissertation]. New Zealand: Auckland University; 2003 [cited 2010 June 18]. [334 p]. Available from: http://researchspace.auckland.ac.nz/handle/2292/1940.

[10] American Wind Energy Association (AWEA). The US Small Wind Turbine Industry, Roadmap, A 20-Year Industry Plan for Small Wind Turbine Technology. Golden, Colorado: National Wind Energy Center; 2002 [Cited 2010 June 12]. [47 p]. Available from: http://www.awea.org/smallwind/documents/31958.pdf

[11] Foreman KM. Size Effects in DAWT Innovative Wind Energy System Design. Solar Energy Engineering 1983;105: 401-407.

[12] Foreman KM. Diffuser Augmented Wind Turbine. Solar Energy 1978; 20:305-311.

[13] Gilbert BL, Foreman KM, Experiments with a Diffuser-Augmented Model Wind Turbine. Journal of Energy Resources Technology 1983;105:46-53.

14] Foreman KM. Preliminary Design and Economic Investigations of Diffuser Augmented Wind Turbines (DAWT). Golden, Colorado: Solar Energy Research Institute; 1981[cited 2010 May 22]. [36 p]. Available from: http://www.nrel.gov/docs/legosti/old/98073-1A.pdf.

[15] Igra O. Research and Development for Shrouded Wind Turbines. Energy Conversion and Management 1981;21:13-48.

[16] Bet F, Grassmann H. Upgrading Conventional Wind Turbines. Renewable Energy 2003;28:71–78.

[17] Tokuyama H, Ushiyama I, Seki K. Experimental Determination of Optimum Design Configuration for Micro Wind Turbines at Low Wind Speeds. Wind Engineering 2002;26(1):39-49.

[18] Hansen MOL, Sorensen NN, Flay RGJ. Effect of Placing a Diffuser Around a Wind Turbine. Wind Energy John Wiley & Sons, Ltd. 1999;**3**:207–213.

[19] Abe K, Nishida M, Sakurai A, Ohya Y, Kihara H, Wada E, Sato K. Experimental and Numerical Investigations of Flow Fields Behind a Small Wind Turbine with a Flanged Diffuser. Journal of Wind Engineering and Industrial Aerodynamics 2005; 93:951–970.

[20] Velte CM, Hansen MOL, Jonck K. Experimental and Numerical Investigation of the Performance of Vortex Generators on Separation Control. Journal of Physics: Conference Series. IOP Publishing 2007[cited 2010 June 4];**75:[**11 p]. Available from: http://iopscience.iop.org/1742-6596/75/1/012030.

[21] Logdberg O, Angele K, Alfredsson PH. On the Robustness of Separation Control by Streamwise Vortices. European Journal of Mechanics B/Fluids 2010;29:9-17.

[22] Fletcher CAJ. Computational Analysis of Diffuser-Augmented Wind Turbines. Energy Conversion and Management 1981; 21:175-183.

[23] Leschziner MA. Modelling Turbulent Sseparated Flow in the Context of Aerodynamic Applications. Fluid Dynamics Research 2006; 38:174–210.

[24] Torresi M, Camporeale SM, Strippoli PD, Pascazio G. Accurate Numerical Simulation of a High Solidity Wells Turbine. Renewable Energy 2008;33: 735–747.

# APPENDIX A: TURBULENCE MODEL COMPARISON

The STAR CCM+ Spalart-Allmaras, S-A, Turbulence solver was used to compare to the results of the K-ε turbulence analysis'. The K-ε model is a robust model in a wide variety of flow applications and was chosen for the primary solver for this study due to the author's familiarity and comfort level with it. The S-A Turbulence model is recommended for aerodynamic flows around curved shapes such as turbine blades and airfoils [23]. It is also known as well suited for primarily attached flows in which separation effects are minimal [24].

The S-A Turbulence model showed minor improvements in $C_p$ as compared to the K-ε model. The peak value of $C_p$ for the S-A model was 1.568 compared to the peak value of 1.553 for the K-ε model, see Figure B.1. This is a difference of only 0.9% at the highest $C_p$ values. The most noticeable differences occurred at non-optimum $C_t$ values. For these non-optimum cases the S-A model predicted a $C_p$ up to 8.7% higher than the K-ε model. This can be explained by the different methods that these two models predict separation of flow and the S-A model's intended use for largely attached flows [23]. For the purposes of this study in which the peak $C_p$ values are the values of interest, the K-ε turbulence model compares very closely with the more specialized S-A model. In addition it provides a more conservative estimate of $C_p$ based on its earlier prediction of separated flow and appears to be a valid choice.

## A.1 Figures

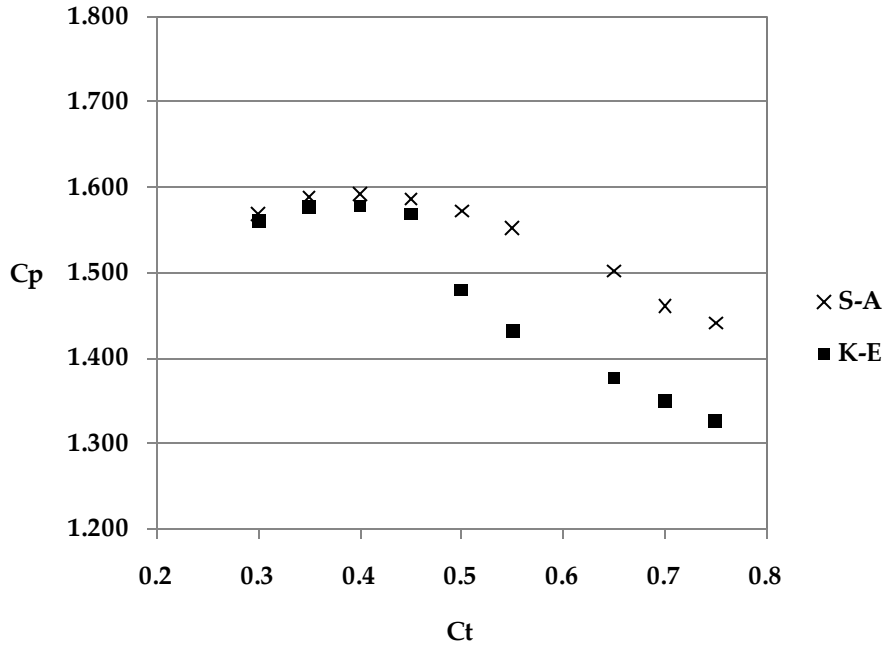


**Figure A.1: Comparison of Power coefficient, $C_p$, versus Thrust Coefficient, $C_t$, using K-Epsilon and Spalart-Allmaras Turbulence Models**

# APPENDIX B: COMPARISON TO PREVIOUS TESTS

One of the most important elements of an analytical study is correlation back to empirical results or theory. In this study three separate cases were analyzed and compared back to results from previous tests and theory. The first of these comparative studies was a bare turbine. A bare turbine was simulated using the same filter element that was used in the various diffuser studies. The only difference was the lack of a diffuser. The second case was a simulation examining the Grumman study diffuser with a 2.78 EAR and LTDR of 0.715. The third case looked a diffuser from the Auckland study. This diffuser had an EAR of 3.0 and a LTDR of 0.488. All of the cases used the same test setup as the other phases of this study. The details of this test setup can be found in Chapter 4.

## B.1 Bare Turbine

The first case looked at a bare rotor. The bare rotor was simulated using a filter modeled as a porous media. The thrust coefficient of this filter was varied. Area averaged velocity at the upstream plane of the filter. Area-averaged pressures were recorded for the upstream and downstream planes of the filter to give a pressure difference across the rotor. Plugging these measurements into Equation 4.1 yielded a power coefficient. The resulting power coefficients at various thrust coefficients were recorded for the filter element representation of a rotor. These results were then compared back to the theoretical relationship.

$$C_p = \frac{1}{2} C_t \left(1 + \sqrt{1 - C_t}\right) \quad \text{(B.1)}$$

The results of this comparison were plotted in Figure B.1. The difference between the theoretical values based on actuator disc theory and the $C_p$ values based on area averaged velocity and pressure difference was less than 1.7% for all values of $C_t$.

## B.2 Grumman Diffuser

The second case examined the Grumman DAWT. This was modeled at the same scale as the actual test, see Figure B.2. The Diffuser model was created based on figures from the Grumman paper [13]. The rotor diameter was 0.46m and the wind tunnel velocity was 36 m/s, see Figure B.3. There have been some questions about the validity of the power coefficients that were published in the Grumman paper [9]. Upstream pressure readings were taken on leading edge of the diffuser. This would yield a higher pressure than that seen at the leading plane of a rotor and would thus give the impression of a greater than actual power coefficient. The peak $C_p$ value in this CFD study was 1.12 at a $C_t$ of 0.95. As presented in the Grumman paper this value of $C_p$ would be divided by the Betz limit to yield an Augmentation level of 1.89. The results of the study are plotted in Figure B.4. Grumman estimated an Augmentation level of 2.75. Phillips evaluated the same Grumman diffuser and estimated an Augmentation level of 1.85 [9]. This correlates closely with value found in this CFD study, with a difference of only 2.1%.

## B.3 Auckland Diffuser

The third case looked at the diffuser developed in the Auckland study, see Figure B.5. This study used a 0.48 m diameter diffuser with a wind tunnel velocity of 10.5 m/s, see Figure B.6. The peak $C_p$ value in this CFD study was 1.12 at a $C_{t,\infty}$ of 0.98. As presented in the Auckland paper this value of $C_p$ would be divided by the Betz limit to yield a peak augmentation level of 1.88. The results of the study are plotted in Figure B.7. Phillips estimated an Augmentation level of 1.73 based on pressure and velocity readings [9]. In this case, the CFD results yielded a higher augmentation, with a difference of 8.7%. This slightly exaggerated performance is not a cause for concern given the lack of design details available for the Auckland Diffuser. The CFD study used a diffuser design that was modeled to represent the Auckland design based on solely on incompletely dimensioned diagrams.

B.4 Figures

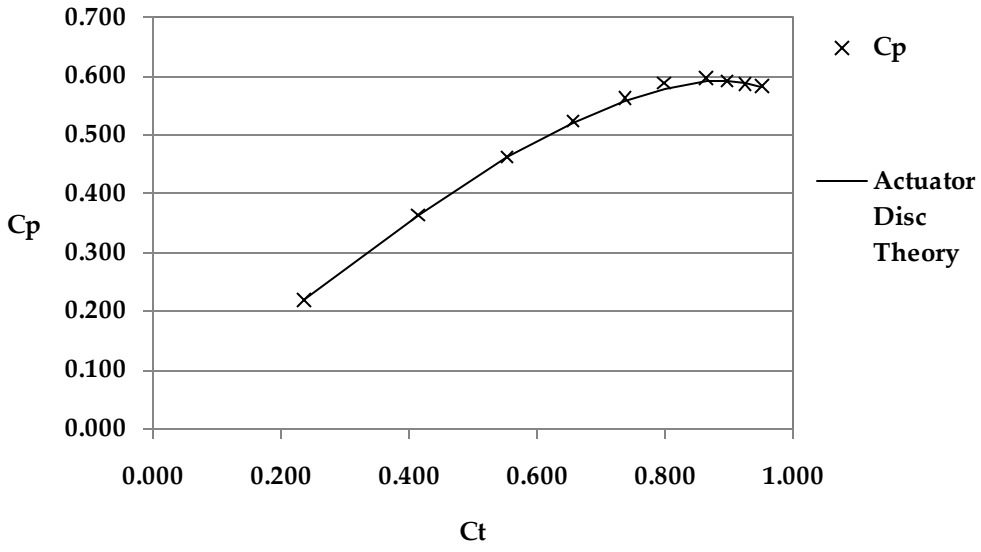


**Figure B.1: Comparison of Theoretical and Analytical Models of a Bare Wind Turbine**

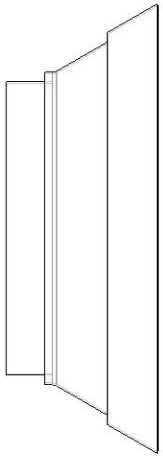

**Figure B.2: Author's interpretation of Grumman Diffuser**

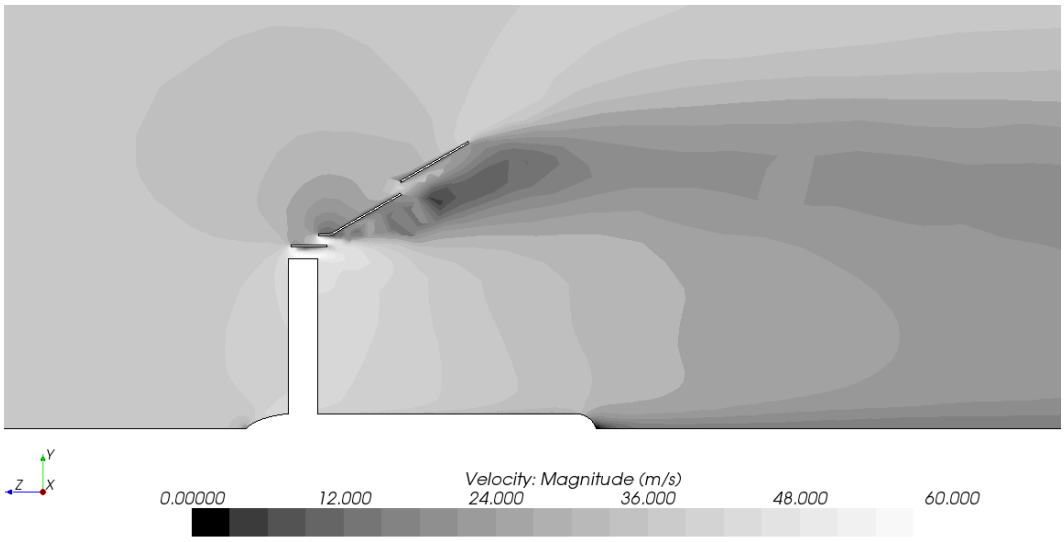


**Figure B.3: Velocity Gradient Plot of Grumman Diffuser Showing Large Area of Separated Flow**

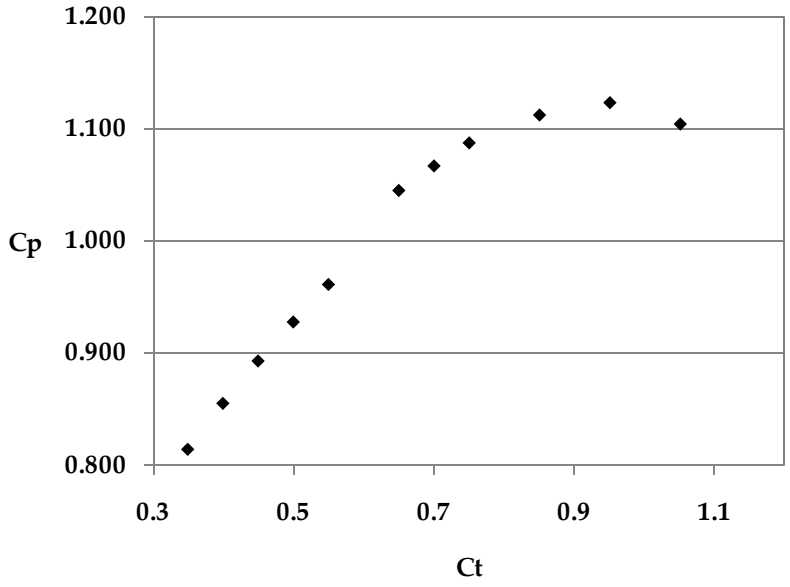


**Figure B.4: CFD Results for Variation of Power Coefficient with Thrust Coefficient for Grumman Diffuser Design**

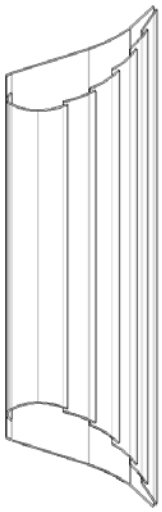

**Figure B.5: Author's Interpretation of Auckland Diffuser**

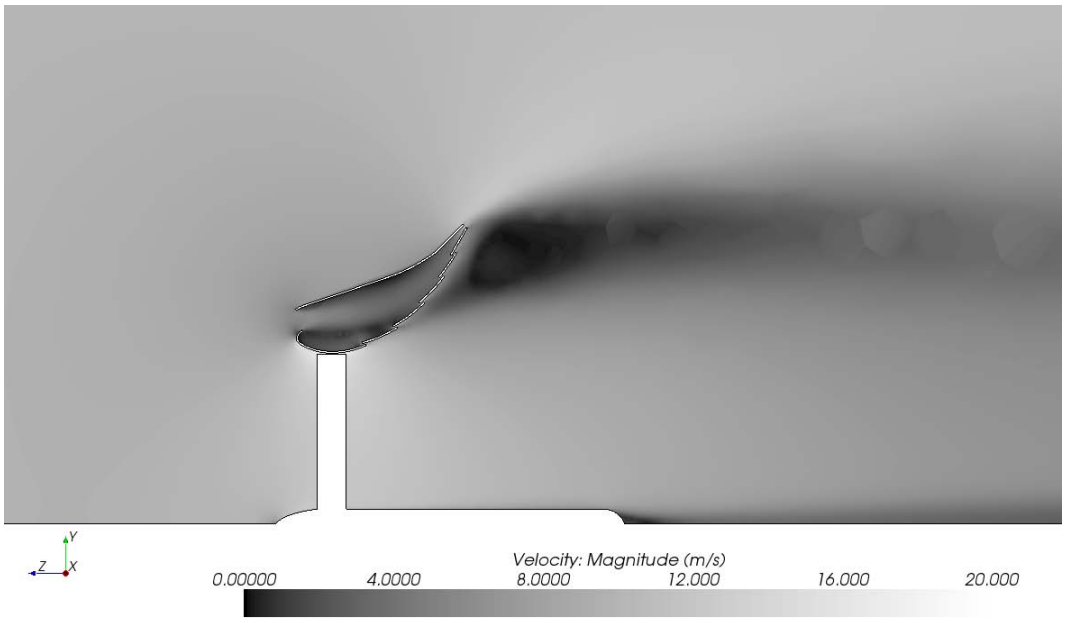


**Figure B.6: Velocity Gradient Plot of Auckland Diffuser Showing Large Area of Separated Flow**

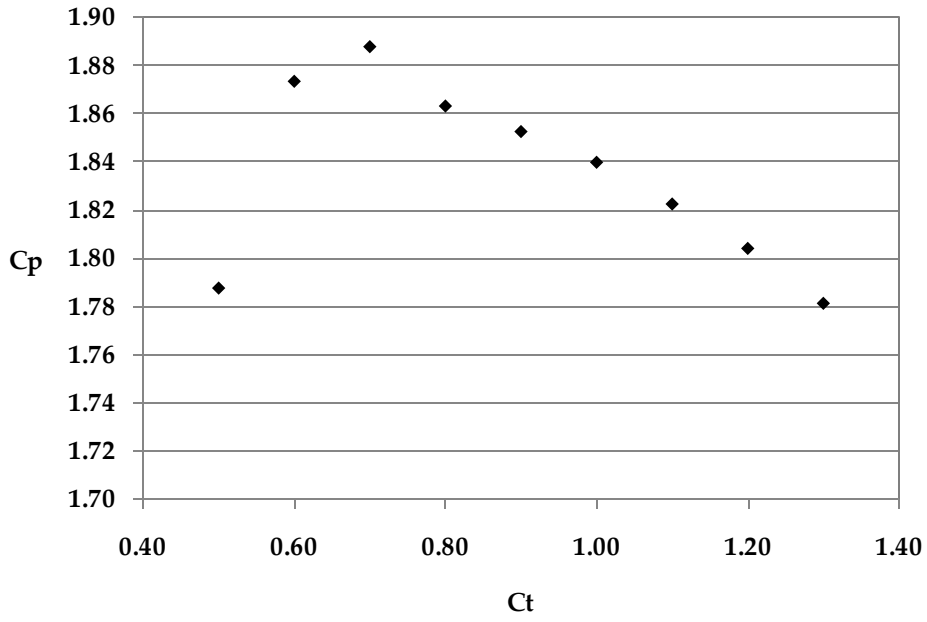


**Figure B.7: CFD Results of Variation of Power Coefficient with Local Thrust Coefficient for Auckland Design**

## B.5 Tables

**Table B.1: Results of Comparison between Theoretically Predicted $C_P$ and CFD Results for a Standard HAWT**

| $C_t$ | $C_{P,CFD}$ | $C_{P,Theory}$ | Difference (%) |
|---|---|---|---|
| 0.236 | 0.219 | 0.221 | 0.831 |
| 0.414 | 0.364 | 0.365 | 0.308 |
| 0.553 | 0.462 | 0.461 | 0.276 |
| 0.656 | 0.524 | 0.520 | 0.763 |
| 0.737 | 0.564 | 0.557 | 1.224 |
| 0.799 | 0.588 | 0.579 | 1.706 |
| 0.863 | 0.596 | 0.591 | 0.875 |
| 0.896 | 0.592 | 0.592 | 0.051 |
| 0.925 | 0.588 | 0.589 | 0.208 |
| 0.950 | 0.585 | 0.581 | 0.619 |